Analysis of Cobalt Deposition Mechanisms in the Primary Coolant System of PWRs

Technical Report

Analysis of Cobalt Deposition Mechanisms in the Primary Coolant System of PWRs

TR-109006

WO4225

Final Report, September 1997

Prepared by
Korea Electric Power Research Institute
103-16, Munji-Dong
Yusung-Gu, Taejon
305-380 Korea

Principal Investigator
S. Shin

Prepared for
Electric Power Research Institute
3412 Hillview Avenue
Palo Alto, California 94304

EPRI Project Manager
H. Ocken
Low Level Waste, Chemistry and Radiation Control

Nuclear Power Group

DISCLAIMER OF WARRANTIES AND LIMITATION OF LIABILITIES

ORGANIZATION(S) THAT PREPARED THIS REPORT

Korea Electric Power Research Institute

ORDERING INFORMATION

Requests for copies of this report should be directed to the EPRI Distribution Center, 207 Coggins Drive, P.O. Box 23205, Pleasant Hill, CA 94523, (510) 934-4212.

REPORT SUMMARY

Deposition of Cobalt-60 (Co-60) on out-of-core components is the primary cause of radiation exposure to plant maintenance personnel and is thus central to reducing worker exposure. This report analyzes deposition of Co-60 in the primary system of PWRs through equations which address the corrosion behavior of structural alloys, the transportation of corrosion products, and the activation of cobalt in the reactor core. Use of this approach reveals that the highest level of deposited activity is on stainless steel in the hot leg side of the primary circuit.

Background

Because Co-60 is the largest contributor to shutdown radiation fields, many efforts have been undertaken throughout the industry to develop analytical approaches that address various aspects of Co-60 activation and deposition. EPRI believes that alternative formulations could provide fresh insights into dealing with complicated exposure processes.

Objective

To develop an analytical approach that addresses corrosion product release, transport, activation, and deposition in order to predict the Co-60 inventory in PWR primary circuits.

Approach

The principal investigator reviewed EPRI's previously developed rate constants for the transportation kinetics of corrosion products. Using this information, he developed a deposition model and formulated a possible transport mechanism of corrosion products in the primary coolant system. Based on the transport mechanism, he developed mathematical expressions for the thicknesses of oxide films formed on structural materials and the specific activities of these films. Finally, by using an EXCEL spreadsheet to solve those equations, he calculated the total Co-60 inventory deposited in the primary coolant system.

Results

The model assumes that corrosion release from structural alloys obeys linear corrosion kinetics. Following are other key assumptions of the model:

- The release of corrosion products is governed by ionic dissolution, and the dissolution rate is proportional to the thickness of the oxide films. The rate constants are 4.16×10^{-7} s-1 for stainless steel and 5.56×10^{-8} s-1 for alloy 600.

- Deposition of crud onto the fuel results from particulate deposition, and activated crud is released as particulates by erosion. The rate constants are 7.94 $x10^{-4}$ m/s for deposition and 1.83$x10^{-6}$ s-1 for release.
- The incorporation of activated corrosion products from the coolant into oxide films is governed by the deposition of ionic species. Deposition rate constants are 8.53$x10^{-4}$ m/s for stainless steel and 2.28$x10^{-5}$ m/s for alloy 600.

This approach was used to calculate the thickness of deposits on structural alloys, the specific activity of crud, and the inventory of Co-60 in the primary system. Reasonable agreement was obtained with published data. Key results follow:

- The thickness of oxide films formed on stainless steel in the hot leg side was 14.9 g/m^2 in the steady-state after three operating cycles. The thickness of oxide films formed on alloy 600 was about one-fourth of that formed on stainless steel.
- Oxide films formed on stainless steel in the hot leg side showed the highest specific activity of 4.33$x10^{7}$ Bq/g. The lowest specific activity in oxide films formed on structural materials was found in alloy 600 used in the cold leg side—9.77$x10^{5}$ Bq/g in the steady state.
- A predicted value of the total inventory of Co-60 in the out-of-core primary coolant system was 466 GBq—143 GBq in the hot leg side and 323 GBq in the cold leg side. The most important radiation sources in the out-of-core primary coolant system were the main coolant pumps.

EPRI Perspective

By assuming a constant corrosion rate for primary system alloys, a comparatively simple approach was developed for analyzing activity transport and deposition on PWR primary system surfaces. This approach is useful for calculating these quantities during steady-state operation. Additional analyses would be required to expand this approach to handle activity transport issues during startup and shutdown transient conditions and to account for the effects of different surface treatments on deposited activity.

TR-109006

Interest Category

Radiation field control

Key Words

Radiation buildup
PWR

ABSTRACT

Deposition of ^{60}Co on out-core components is the main cause of radiation exposure of plant personnel during maintenance work. Therefore, the understanding of deposition mechanism of ^{60}Co in the primary coolant system is very important to find ways to reduce the radiation worker's exposure. In order to develop a deposition model of ^{60}Co in the primary coolant system, the previous work regarding ^{60}Co buildup in the primary coolant system of PWR was reviewed. Based on the published data, a possible transport mechanism of corrosion product was suggested.

Linear kinetics was assumed to evaluate the cobalt input from structural materials into the coolant by corrosion. By assuming that the release mechanism of corrosion products from oxide films into the coolant is governed by ionic dissolution reaction, and the dissolution rate is proportional to the thickness of oxide films, release rate constants, 4.16×10^{-7} s^{-1} for stainless steel and 5.56×10^{-8} s^{-1} for Inconel-600, were obtained. Particulate deposition of crud from the coolant onto fuel rod and particulate release of activated crud by erosion from the fuel rod into the coolant were assumed from the evidence found in the published data. The rate constants obtained here are 7.94×10^{-4} m/s for deposition kinetics, and 1.83×10^{-6} s^{-1} for release kinetics. The incorporation of activated corrosion products from the coolant into the oxide films formed on structural materials was assumed to be governed by the deposition of ionic species. Deposition rate constants of 8.53×10^{-4} m/s for stainless steel and 2.28×10^{-5} m/s for Inconel-600 were obtained. However, particulate deposition from the coolant into the oxide films was also included to explain several findings from the previous work.

Based on the transport mechanism of corrosion products in the primary coolant system, mathematical expressions for the thicknesses of oxide films formed on structural materials and the specific activities of cruds were obtained. By using an EXCEL spreadsheet, the total ^{60}Co inventory deposited in the primary coolant system was calculated. The results showed quite good agreement with the findings from in-reactor loop experiments and from field measurements.

CONTENTS

FIGURES

TABLES

1. INTRODUCTION

Corrosion products in the primary coolant system of a pressurized water nuclear reactor can produce several kinds of operational problems due to deposition on various surfaces in the system. Hydraulic resistance can be caused by the increased surface roughness or reduced coolant channel dimensions which can lead to increased pressure drop across the core. Also, reduced dimensions of orifices such as in valves, re-circulation pumps, emergency cooling water supply lines or in 'dead-leg' connections, can lead to reduced flows.[1)]

Thermal resistance increased by the crud deposited on fuel cladding can lead to a decrease in the heat transfer capability between the fuel element and the coolant. It renders possible eventual fuel rupture and burn-out.

Reactivity loss of the core which can be caused by an increase in fuel temperature provides also the possibility of additional reactivity loss in systems operated with chemical shim control, e. g. the absorption of boron in the crud leading to nuclear poisoning of the fuel, and axial offset anomaly.

Finally, corrosion product radioactivity which accumulates on out-of-core pipework and equipment can be a major source of radiation to personnel carrying out maintenance tasks. In the case of planned maintenance at shut-down periods the longer-lived species such as ^{60}Co ($t_{½}$ = 5.3 y) and ^{54}Mn ($t_{½}$ = 312d) are the limiting factors, but for "trouble-shooting" corrective maintenance the shorter-lived (few day and even hour half-lived) species will determine how long the shut-down will last. In this report, most of effort will be concentrated on the analysis of ^{60}Co transport in the primary coolant system of PWRs.

There are some typical characteristics in the PWR primary system which should be considered when analyzing the transport process of crud.[4)] First of all, the primary coolant system is the essentially closed coolant circuit. Therefore, there are no significant external sources of corrosion products in PWRs. The presence of different constructional materials, e.g., the large areas of high nickel alloys used for

steam generators makes the release and deposition process complicated. The temperature variation around the coolant circuit provides a driving force for the transport of crud in the circuit. This variation can be as much as 40℃ (~280 to 320℃) in the PWR coolant system compared with <10℃(274 to 280℃) in BWRs. The difference between core inlet and outlet temperatures can determine the solubility of material species carried by the PWR coolant and hence the potential for in-core deposition. The various coolant chemistry should be also noted. The use of coordinated lithium/boric acid levels for pH control aims to minimize the in-core deposition, and hence the activation of corrosion products.

In order to evaluate the buildup rate of ^{60}Co in the out-core system, and thereby the radiation level of the system, it is necessary to analyze the corrosion and wear rate of ^{59}Co, the parent nuclide of ^{60}Co, from the in-core and out-core components. Bergmann et al. have evaluated the cobalt sources in Westinghouse-designed three- and four-loop plants, and summarized the corrosion rates of different constructional materials at reactor coolant conditions from the previous works.[16] At the same time, Young et al. have implemented a cobalt source identification program for Combustion Engineering-designed PWRs.[17] They also presented typical corrosion rates and wear rates for different materials used in the PWRs. Bergmann et al. have also summarized some experimental results for release rates from the oxide film formed on the surface of different materials into coolant. Balakrishnan and Lister have tried to express the growth rate of oxide films as an mathematical expression for each material.[14,19]

Released ^{59}Co absorbs a neutron, and transforms into ^{60}Co in the core. Because of the long half life of ^{60}Co, it becomes the most significant contributor to the occupational radiation exposure with time. Many efforts have been exerted to determine the produced activity of ^{60}Co from the core. For example, Solomon and Roesmer measured the compositions of crud on the fuel elements from Point Beach NPP and Beznau NPP, and analyzed the residence time of ^{59}Co in the core.[10] The average composition and specific activity of crud collected from steam generator tubes were analyzed by Bergmann and Roesmer, Bridle et al., and Song et al.[20,21,22] And Balakrishnan and Allison have analyzed the rate constants for some of the transfer processes involved in the contamination of the primary heat circuit in

water-cooled nuclear power reactors from the in-reactor loop experiment results.[7]

Deposition of ^{60}Co produced from the neutron absorption of ^{59}Co in the out-core components is the main cause of radiation exposure of plant personnel during maintenance work. In order to find a way to reduce the buildup of ^{60}Co in the primary coolant circuit, several researchers have tried to explain the deposition mechanism of ^{60}Co in the out-core components. Lister has developed a transport model of radioactive corrosion products in high temperature water for the isothermal steel surfaces and non-isothermal steam generator tubing.[8,12,19] Lister, Davidson, and Ocken have also analyzed the transport process of corrosion products in light water reactors.[23] In order to examine the effect of pH on the deposition of ^{60}Co, in-pile loop studies were carried out by Driscoll et al.[28] The effect of surface treatments on the buildup of radioactivity has been recently examined through several projects carried by EPRI.[29,30,31,32]

The goals of this report are:

- review the previous work regarding ^{60}Co buildup mechanism in the primary coolant system of PWRs,
- analyze and provide a possible transport mechanism of corrosion products in the primary coolant system for the analysis of deposition of ^{60}Co, and
- provide a simple way to predict the inventory of ^{60}Co in the primary coolant system of PWR.

In chapter 2, corrosion behavior of structural materials used in PWRs will be discussed, and a simple and conservative corrosion mechanism will be proposed for the evaluation of ^{60}Co inventory in the primary coolant circuit of a PWR. The release of cobalt from the oxide films that form on the different structural materials into the coolant will be analyzed in chapter 3 based on the published data from previous work. From the measured radiochemical data for fuel deposits and particulates in the coolant, an in-core deposition and release model will be established (chapter 4), and out-core deposition mechanism will be analyzed in chapter 5. The effect of water chemistry, heat transfer, and surface treatment on the deposition of ^{60}Co in the primary coolant system will be reviewed, and a

possible way to explain the effect will be suggested. Finally, ^{60}Co inventory deposited in the primary coolant system based on the proposed model will be evaluated by using an EXCEL spreadsheet, and a comparison between the published data and the data obtained from the model will be performed in chapter 6.

2. CORROSION BEHAVIOR OF STRUCTURAL MATERIALS USED IN PWRS

2-1 Typical Primary Coolant System of a PWR

In pressurized water reactor, the fission heat generated in the core is transferred to the water coolant without bulk boiling occurring. This implies there are two circuit heat transfer systems in PWRs: a primary coolant system which consists of the core and one side of steam generators, and a secondary cooling system which consists of the steam side of the steam generators, turbines, and a condenser. The primary coolant is pressurized to ~14 MN/m^2 to prevent boiling at ~300 ℃, and is usually dosed with an alkali hydroxide to control the coolant pH at 10~10.5 as measured at room temperature. The coolant is pumped around circuit and linear flow rates in the core are approximately in the range of 6 to 9 m/s in PWRs.

The main source of corrosion products is the structural materials of the primary coolant circuit. The corrosion behavior of structural materials determines the rate of corrosion product input to the coolant system, thereby the production of ^{60}Co in the core. The chemistry condition of coolant has an important role in deciding the corrosion behavior. Table 2-1 provides the typical chemistry specification for PWR coolant.[4] As shown in the table, the coolant pH allows the wide variation of 5.4 to 10.6 depending on the operating condition, even though the pH is now controlled to meet the strict guidelines in the most PWRs to reduce the corrosion product input to the coolant. Lower pH can increase the corrosion rate of structural materials used in PWRs.

The total input of corrosion products into the coolant system is determined by the type of materials, the area contacting with the coolant, and the corrosion rates and wear rates of the materials. Table 2-2 identifies the type of materials and the area contacting with the coolant for a typical 1,000 MWe PWR. In this table, it is apparent that Zircaloy-4 is the major material which contacts with the coolant in the core, and Inconel-600 is the major possible source of corrosion products in the

Table 2-1

Typical Chemistry Specification for PWR Coolant

Boron	Variable[a] 0 - 2500 ppm B
^{7}LiOH	0.7 - 2.2 ppm Li
pH value at 25℃	Variable[b] 5.4 - 10.5
pH value at ~300℃	~5.6 - 7.5
Dissolved hydrogen	15 - 50 cm^3 (NTP)/kg
Dissolved oxygen	< 0.07 cm^3 (NTP)/kg
Chloride	< 0.15 ppm
Fluoride	< 0.15 ppm
Crud (suspended metal oxides)	< 1 ppm
Silica	< 0.2 ppm
Al, Cu or Mg	< 0.1 ppm each
Electrical conductivity at 25℃	4 - 80[a] μS/cm

a. Reduces during fuel cycle for reactivity control.
Peaks during shutdown (cold)

b. Variation controlled by ^{7}LiOH concentration for a specific boron level.

Table 2-2

Alloys Used in Primary Coolant System of Four-Loop PWRs

Components		Area Contacting with the Primary Coolant (dm^2)[a]				
		SS 304[b] (Corrosion)	Inconel-600[c] (Corrosion)	Stellite-6 (Corrosion)	Stellite-6[d] (Wear)	Zircaloy-4[e]
Steam Generator		6,911	1,792,933			
Main Coolant Piping		20,711				
Reactor Vessel		21,359				
Pressurizer		12,569				
Heat Exchanger (High Temp.)		8,264				
Heat Exchanger (Low Temp.)		10,366[f]				
Main Coolant Pump		21,486		272	0.7	
CRDM Parts		29,485	3,246	305	8.2	
Reactor Vessel Internal		109,490		61	1.3	
Fuel Assembly		55,474	72,833			723,396
Valves				285	17.8	
Total	In-Core	215,808	76,079	366	9.5	723,396
	Out-Core	80,307	1,792,933	557	18.5	
	Total	296,115	1,869,012	923	28	723,396

a. These data were summarized from the data for Trojan NPP given in Ref. 16.

b. It includes SS 304, SS 308, SS 403, and SS 410.

c. It includes Inconel-600 and Inconel-718 which is used in fuel assembly.

d. The area was evaluated by using 50 mg/dm^2-mo of wear rate and the cobalt input given in Ref. 16.

e. No corrosion for Zircaloy-4 is assumed. The area is important for the evaluation of ^{59}Co deposited on the fuel rod.

f. Adjusted by considering operation time of heat exchangers.

out-core components.

The wear rate of hardfacing alloy depends on the operation mode of the component, friction factor caused by flow condition, and other environmental conditions. It implies that the wear rate may differ from component to component depending on the operation conditions. Note that the contribution to the cobalt input into the coolant by wear is not negligible compared to that caused by corrosion. According to the cobalt source data evaluated for Westinghouse- designed plants, about 10 % of cobalt input may be caused by the wear of high-cobalt alloys.[16] In fact, it is possible to evaluate the total cobalt input to the coolant by using the data given in Ref. 16. However, the constant wear rate is assumed for the convenience of analysis in this report. This subject will be discussed in more detail later.

The cobalt source entering to the coolant released by wear from the hardfacing alloys has the different form from the corrosion products. Rather than an oxide, it may be the tiny debris of base metal itself. Therefore, it is hard to say that wear products will follow the same deposition mechanism onto the fuel rod or release mechanism from the fuel rod. However, it is assumed for the wear products to be small enough to undergo prompt corrosion in the coolant as soon as it is released. Under this assumption, the wear products will be treated the same as the corrosion products in this report.

2-2 Investigation of Corrosion and Wear Data

In order to determine the cobalt from structural materials into the coolant, it is very important to know the level of ^{59}Co contained in the base metals. The level of ^{59}Co in the base metal depends on the type of alloy, the manufacturer of the materials, and even the specific batch used. Even though it is true that the cobalt input into the coolant should be based on the plant data, the cobalt contents and densities for the structural materials appeared in Ref. 23 were adopted as reference values in this report for the general evaluation of deposition mechanism of ^{60}Co in the primary system of PWRs. Table 2-3 provides the data of cobalt contents and densities for the materials used in PWRs.

The corrosion rate of base materials and the release rate of corrosion products from the oxide film formed on the surface of base materials are the most important factors governing the input of cobalt into the primary coolant, thereby the radiation level in the out-core components by the accumulation of ^{60}Co which is produced by the neutron activation of ^{59}Co in the core. A review of some corrosion data was conducted to determine representative corrosion rates for the materials.

Table 2-3

Cobalt Content and Density
of Structural Materials Used in PWRs

Material	Density, ρ (g/cm^3)	Fraction of ^{59}Co f (g/g)
Stainless Steel	7.9	2×10^{-3}
Inconel	8.51	5×10^{-4}
Stellite	8.83	0.55

Table 2-4 shows the corrosion rate and release rate for the plant construction materials that appears in the literature. As shown in this table, the data reveal large deviations depending on the investigators and the experimental conditions. It is unlikely to define a reliable value for the corrosion rate or release rate. However, it is possible to find some interesting consistencies between the data. Generally, the corrosion rate of Inconel-600 generally appears to be higher than that of stainless steel except for the data from Ref. 1. Considering that the area of Inconel-600 which contacts with the primary coolant is larger about 6 times that of stainless steel, the total weight of metal oxides forming on the primary coolant system should be dominated by the corrosion of Inconel-600. Moreover, the data show the higher release rate of Inconel-600 than that of stainless steel. It implies that the input of corrosion products into the coolant will be governed by the corrosion product input from Inconel-600. Therefore, the level of ^{60}Co accumulated on the out-core components can be greatly affected by the content of cobalt contained in Inconel-600.

Not enough data show the relationship between the corrosion rate and the test time. However, the data reported in a reference quoted in Ref. 16 indicates that the corrosion rate may be time-dependent, and may decrease with time. Some authors have tried to describe the corrosion rate with the mathematical formula from the radiation level accumulated on the stainless steel and the steam generator tubing. It will be discussed in the following section.

The corrosion rate of Stellite-6 is very important because of the higher cobalt content, even though the area contacting with the primary coolant is relatively small compared to that of other materials. Unfortunately, we have a limited information on the corrosion rate of Stellite. Some experimental results referenced in Ref. 16 show that the corrosion rate of Stellite is a bit lower than that of Inconel-600. However, the same corrosion rate as that for Inconel-600 is generally adopted for Stellite-6.

A few data are available regarding the wear rate of hardfacing alloys. As mentioned earlier, it is impossible to find a reasonable value for the wear rate, because the wear rate depends heavily on the operation conditions of the equipment

Table 2-4

Corrosion and Release Rate
of Plant Construction Materials Used in PWRs

Test Condition	Test Time (Month)	Corrosion and Release Rate (mg/dm^2-mo)						Ref.
		SS 304		Inconel-600		Stellite-6		
		Corrosion	Release	Corrosion	Release	Corrosion	Release	
Plant Condition	-	2.5-5.0	0.6-1.5	2.5	1.0-1.5	5-25	5-25	1
300℃, pH=6.9, 1,000 ppm B	-	2	0.1	5	0.25	5	0.25	17
550-600°F, Boric Acid+Alkali	-	1.8	0.9	5.8	3.9	3.0	1.5	16
315℃, 10^{-4}M LiOH	2	15.1	8.6	24.1	3.5			Ref. 8 in Ref. 16
315℃, 10^{-4}M KOH	9.2	4.0	2.0	15.6	6.4			
300℃, pH=5.6-7.2 LiOH chemistry	> 2	-	2.0	-	4.3-12.8			Ref. 6 in Ref. 16
315℃, pH=10 LiOH or KOH	2 to 5	2.0	-	4.3	-			Ref. 7 in Ref. 16
315℃, pH=5-9.5	1					2.2-4.4		Ref. 17 in Ref. 16

or the component. For example, the wear rate from the hardfacing alloys used in the valve stem is determined by the frequency of valve operation.

Therefore, in principle, the wear rate should be evaluated on the basis of operation mode of each component. That is why measurements of actual wear of components were used in the cobalt source evaluation project for the Westinghouse-designed plants conducted by EPRI, where available. However, a constant wear rate will be assumed for all components in this report to simplify the analytical approach. Instead of using different wear rates, the area of undergoing wear given in Table 2-2 was evaluated to compensate the different wear rates of components from the field measurement data if available. For instance, the area was determined to give the measured wear rate from a constant rate. A constant wear rate of 50 mg/dm^2-mo given in Ref. 17 was used for the analysis of cobalt input from Stellite-6 in this report.

2-3 Corrosion Mechanism of the Structural Materials

2-3-1 General Characteristics of Oxide Film

It is well known that there is a thermodynamic driving force for corrosion to proceed. The oxidation and reduction reactions for a corrosion cell depend on each other, although they are often treated as independent processes. For instance, the overall corrosion mechanism of low alloy steels can be given by

$$Fe \rightarrow Fe^{++} + 2e^{-} \quad \text{(anodic reaction)}$$

$$2e^{-} + 2H_2O \rightarrow 2OH^{-} + H_2 \quad \text{(cathodic reaction)}$$

$$2e^{-} + \tfrac{1}{2}O_2 \rightarrow 2OH^{-} \quad \text{(cathodic reaction)}$$

In the above reactions, the latter reaction takes place in the presence of oxygen. Ferrous hydroxide formed by the corrosion reactions has high solubility due to the following reactions,

$$Fe(OH)_2 \rightleftharpoons FeOH^{+} + OH^{-}$$

$$FeOH^{+} \rightleftharpoons Fe^{2+} + OH^{-}$$

Therefore, ferrous oxide does not provide a protective layer on the surface of metal. Morphological analysis of the oxide film formed on the surface of base metal in the high temperature water reveals that the oxide film formed on the low alloys has the structure of magnetite(Fe_3O_4) or hematite(α-Fe_2O_3). In general, corrosion films that form on the surface of base metal consist of two layers; an outer layer of hematite which is loosely attached, and an adherent inner layer.

The process of film development is dependent on the metal surface, water chemistry, and temperature. The magnetite found in the inner layer is thought to be formed through two processes. Conversion reaction of ferrous hydroxide into the magnetite may occur inside the oxide layer. Therefore, it may be converted into magnetite before being released into the coolant as ions by the following reaction.

$$3Fe(OH)_2 \rightarrow Fe_3O_4 + H_2 + 2H_2O$$

Direct formation of Fe_3O_4 from the metal surface is also possible through the reaction between base metal and hydroxyl ions present in the coolant as follows,

$$3Fe + 4OH^- \rightarrow Fe_3O_4 + 2H_2 + 4e^-$$

$$4H_2O + 4e^- \rightarrow 2H_2 + 4OH^-$$

However, considerable doubt still seems to exist as to whether the Fe_3O_4 is formed on the surface or whether it forms in solution and is precipitated later.

In a PWR where no degassing is taking place, the growth of magnetite from solution may occur. The deposits are then black, coarse-grained, reflective and adherent, whereas those formed in neutral water with oxygen present are red, finer-grained, porous and friable and are composed largely of hematite. In general, oxides with a spinal structure (Fe_3O_4 and γ-Fe_2O_3) form a protective film, while α-Fe_2O_3(hematite) having a corundum type of structure is powdery, insulating and less adherent.

In a project conducted to study the incorporation of cobalt into the corrosion product films formed on PWR primary circuit materials (stainless steel 304L, Inconel-600 and Zircaloy-4), characterization of the corrosion product films has been carried out using scanning electron microscopy coupled with energy dispersive analysis using X-rays.[18] The result shows that two layers of oxide film are formed on the surface of base metals. However, the outer layer seems to have the magnetite structure rather than hematite. Some important features of corrosion of stainless steel presented in the report are as follows.

- Corrosion of stainless steel can be characterized by the formation of two oxide layers at the interface between metal and water. The inner layer consists of a chromium-rich oxide resulting from the greater affinity of chromium for oxygen and forms as a uniform layer growing pseudomorphously into the metal.

- Diffusion of iron and nickel through the inner layer results in the formation of

iron-chromium and nickel spinels of the type FeM_2O_4 (M=Cr, Ni) in the outer layer. This layer of oxide grows by re-precipitation from solution in the form of non-uniform crystallite agglomerates. These crystallites can form as thick layers or as single crystallites at scattered sites depending on whether mass transport in the system favors re-precipitation.

- SEM-EDAX analysis results also show that two types of crystal structures can be observed. One is a close packed regular crystal structure adjacent to the metal substrate, which shows a similar concentration of chromium and iron as the base metal. The other is a larger irregular iron-rich crystal structure growing on the surface. Examination of the analytical profile does not show any region of chromium enrichment in relation to iron, i.e. formation of a Cr_2O_3 layer. Diffusion of Fe towards the surface of the film is indicated by the increasing iron concentration, whereas both chromium and nickel decrease towards the surface of the deposit.

- Analysis of oxide film removed from stainless steel indicates the material to be largely Fe_2O_3 with Ni and Cr inclusions as a spinel structure.

Some important features of Inconel-600 corrosion shown in the report (Ref. 18) can be summarized as follows.

- Micrographs of oxide film that forms on the surface of Inconel-600 show that the deposit consists mainly of irregular loosely packed crystallites. Iron enrichment towards the surface is very marked, and is at the expense of nickel and chromium.

- Deposits formed on Inconel-600 are substantially less structured than those that forms on stainless steel. Analysis of oxide film removed from Inconel shows very strong evidence of a mixed oxide composed of iron, chromium and nickel oxides.

There are a few data available regarding the corrosion of Stellite-6. When we consider the effect of Stellite-6 on the cobalt input into the coolant, two remarkable

characteristics of Stellite-6 are likely to be noted. One is the high content of cobalt in Stellite-6. It can cause the high contribution to the total cobalt input into the primary coolant system in PWRs even though it is a much smaller area compared to the other structural materials. The other comes from the relatively small surface area which contacts with the coolant. It means that re-deposition of activated corrosion products onto the surface of Stellite-6 can be negligible, even though it is very important when considering cobalt input to the system.

2-3-2 Corrosion Rate of Structural Materials

In a system saturated with corrosion products, and with no sink for them, it can be assumed that the film growth expression $m(t)$ reflects the corrosion rate. The rate of film growth has been described by various kinetics. In general, four primary oxidation rates have been observed for many metals in various environments. These have been designated as laws but are actually empirical relationships described as linear, logarithmic, parabolic, and cubic. In order to describe the corrosion rate of nuclear structural materials, parabolic kinetics and logarithmic kinetics seem to be generally obeyed.

Parabolic kinetics are the result of a chemical potential gradient of ions, the diffusion of which through the oxide is the rate-controlling step. Therefore, the diffusion flux is inversely proportional to the oxide thickness, i.e., a rate of growth of oxide film is proportional to $t^{-1/2}$, or film thickness is proportional to $t^{1/2}$. This type of oxidation is known to be often observed when thick coherent oxides form, typically at high temperatures where the mobility of ionic components is sufficient to develop such a scale. Metals such as Co, Cr, Fe, and Cu are reported to form these type of scales at high temperature. A parabolic expression for the corrosion rate can be derived as follows,

$$m(t) = \sqrt{K_p\, t} \qquad \text{----------} \quad (1)$$

where K_p : parabolic corrosion kinetic constant, $g^2/m^4 \cdot s$

Logarithmic oxidation kinetics predicts a film growth rate proportional to t^{-1} or film thickness as a function of $\ln t$. A logarithmic expression for the corrosion rate can be derived theoretically by considering the mutual blocking of pores within metal oxides.

$$m(t) = K_\ell \ln(a_\ell t + 1) \quad \text{---------- (2)}$$

where K_ℓ : logarithmic corrosion constant, g/m^2

a_ℓ : logarithmic corrosion kinetic constant, s^{-1}

The kinetic film growth expressions, $m(t)$, for stainless steel were provided by several researchers. They have usually derived the film growth expression from the radiation buildup data on stainless steel. D. H. Lister[19] has suggested the following equations,

$$m(t) = \sqrt{1.73\times10^{-5}\ t}$$

$$m(t) = 0.641 \ln(4.56\times10^{-5}\ t + 1)$$

where $m(t)$ is in terms of oxide(g/m^2) and t is the time in seconds. Both fit the data reasonably well at the initial stage of corrosion.

P. V. Balakrishnan and G. M. Allison[7] have also provided the kinetic expressions for film growth rates on stainless steel. Their equations are

$$m(t) = \sqrt{0.2916 + 5.984\times10^{-6}\ t}$$

$$m(t) = 1.194 \ln(3.90\times10^{-6}\ t + 1)$$

The average corrosion rates (mg/dm^2-day) for 1,000 hrs and 1 yr evaluated from the above two models showed good agreement as shown in the following table.

		Parabolic Model	Logarithmic Model
t = 1000 hrs	Lister's model	1.89 mdd	0.79 mdd
	Balakrishnan's	1.12 mdd	0.78 mdd
t = 1 yr	Lister's model	0.64 mdd	0.13 mdd
	Balakrishnan's	0.38 mdd	0.36 mdd

Film growth expressions for the inner oxide layer formed on Inconel-600 steam generator tubing have been also given by D. H. Lister as follows,[8)]

$$m(t) = \sqrt{3.31\times10^{-7}\ t}$$

$$m(t) = 0.152\ \ln(2.85\times10^{-5}\ t + 1)$$

The average corrosion rates(mg/dm^2-day) for Inconel-600 steam generator tubing obtained from the Lister's model are

	Parabolic Model	Logarithmic Model
t = 1000hrs	0.262 mdd	0.169 mdd
t = 1yr	0.089 mdd	0.028 mdd

From the above comparison data, it is clear that the corrosion rates fit pretty well between both models. Lister's logarithmic models show that the average corrosion rates for 1 year for stainless steel and Inconel-600 are 0.13 mdd and 0.028 mdd, respectively. These values are reasonably agreed with the corrosion data obtained from some experiments. Therefore, it looks quite acceptable to use the above mathematical expressions for the evaluation of corrosion rates. Also these mathematical expressions reflect the time-dependent corrosion behavior observed in the reactor coolant system.

However, there are some drawbacks in using these mathematical expressions for

the evaluation of Co-60 inventory accumulated in the primary coolant circuit. The most important point is that the growth rate of oxide film formed on the surface of base metal does not exactly represent the corrosion rate. In particular, it is true for the open system where the contribution by removal of oxides from the system is significant. In that system, the growth rate of oxide film should be determined from the corrosion rate, release rate, removal rate, and deposition rate. The above mathematical expressions give a long-term corrosion rate of zero, so it is inappropriate for use to explain a reactor primary system where some corrosion products are continuously removed by the purification system and some are continuously produced from the corrosion process. Therefore, it is hard to say that the corrosion kinetics follows the same kinetics as the film growth kinetics.

The second problem may be caused by the fact that the corrosion rate for stainless steel is higher than that for Inconel-600. It doesn't match with the observed phenomena from several experiments, and may result in significant increase in ^{60}Co production rate because of the higher cobalt content in stainless steel. Also, Lister's loop experiments show that the release rate from oxide films changes significantly whenever there is a transient.

It is evident that the corrosion kinetics of metals is controlled by the diffusion of ions through the pores present in the oxide film. Therefore, it is more logical to assume that the corrosion kinetics follows the parabolic expression in a closed loop system at high temperature like the nuclear primary coolant system. However, corrosion products are constantly being removed by the primary coolant purification system from the primary coolant circuit of PWRs. In addition, some corrosion products deposited on the fuel rod will be removed periodically during refuelling from the primary coolant system. Strictly speaking, the nuclear primary coolant system is not a closed system. In this kind of system, it is unlikely for the long-term corrosion rate to be zero. Therefore, the linear kinetics will be assumed as the corrosion kinetics for nuclear structural materials instead of the parabolic or logarithmic mathematical expression. This is a conservative approach for predicting the long-term behaviour in a PWR.

The corrosion rate constants for linear corrosion kinetics, k_c, and the wear rate

constant, k_w, were obtained from the data used in Ref. 17 as follows,

$k_c = 7.716 \times 10^{-8}\ g/m^2 \cdot s$ for corrosion of stainless steel

$k_c = 1.929 \times 10^{-7}\ g/m^2 \cdot s$ for corrosion of Inconel-600 and Stellite

$k_w = 1.929 \times 10^{-6}\ g/m^2 \cdot s$ for wear of Stellite

3. RELEASE MECHANISM OF COBALT SOURCE INTO THE COOLANT

3-1 Overview of Corrosion Product Transport

3-1-1 Review of Corrosion Product Transport Data

In order to understand the release mechanism of cobalt source from the oxide film formed on the surface of structural materials into the coolant, it is necessary to examine all processes that relate to corrosion product transport in the primary coolant circuit of a PWR. Therefore, let's examine the corrosion product transport mechanism in the primary coolant circuit of PWRs, and propose a mechanism for each step of the processes. Then, a mathematical formulation will be derived to analyze the deposition of ^{60}Co in the primary coolant circuit.

Only limited data are available for the crud deposited on the reactor core. Yale Solomon and Josef Roesmer have measured the amount and chemical and radiochemical composition of fuel element crud deposits from Point Beach (WEP) and Beznau 1(NOK) plants. Table 3-1 shows the results of average crud compositions from these plants[10]. As shown in this table, it is apparent that the crud buildup was somewhat greater on the high power assemblies than on those of lower power. The Ni/Fe ratio of the deposits are of particular interest. If all materials corroded at the same rate and the released corrosion products were the same composition as the base metal, the Ni/Fe ratio would be ~9 or 10. It is clear that the ratio found in the crud is much lower than the ratio in the base metal.

Table 3-2 provides the average composition and specific activity of crud deposited on steam generator tubing from Westinghouse-designed plants A to H.[20] Analysis of the crud shows that a mixed Fe, Cr spinel structure was formed on the tubing. The chromium concentration in the crud was high as expected. However, the high cobalt concentration was unexpected because cobalt is known to be released quite

Table 3-1

Average Crud Composition of WEP and NOK Cores[10)]

(wt%±Standard Deviation)

Element	WEP Cycle 1	NOK Cycle 1[b]	NOK Cycle 3	
			Low Power	High Power
Iron	29.6±9.4	47.0±4.1	45.1±19.6	32.3±8.4
Nickel	12.7±4.6	14.4±1.3	21.4±9.6	24.1±8.2
Chromium	1.6±1.0	1.33±0.78	0.78±0.23	2.46±1.09
Manganese	0.06±0.08	0.14±0.06	0.13±0.01	0.19±0.06
Cobalt	0.025±0.08[a]	0.034±0.023	<0.03	0.06±0.02
Nickel/Iron	0.43	0.31	0.47	0.75

a.. Maximum value since most data were below detection limit of 0.005 wt%. The input as value for these points was 0.005.

b. "Post-ignition" values. All others are based on unignited crud weights.

easily as cobalt ions into the solution from the oxide film.[16)] In general, specific activities of short-lived radionuclides might be influenced by the measurement time, so ^{60}Co is the best indicator of radioactivity build-up in the system. However, it is not clear to define a trend in ^{60}Co specific activity found in the Westinghouse plants.

Table 3-3 shows the composition and specific activity of particulate present in the coolant from Doel 3 & 4.[21)] Unlike the composition of fuel deposits, high

Table 3-2

Average Composition and Specific Activity
of S/G Tube Cruds from Westinghouse Plant A~H[20)]

• Chemical Composition

Element	Fe	Ni	Cr	Co	Ni/Fe ratio
Weight Percent	14~22	20~30	20~38	0.24	1.0

• Specific Activity

Plant	EFPY	Specific Activity (μCi/mg)			
		^{55}Fe	^{54}Mn	^{58}Co	^{60}Co
E	1.58	28	-	-	4100
B	1.75	35	13.0	-	5500
D	2.21	24	-	-	4200
G	5.96	25	2.5	-	5900
G	6.84	20	2.2	50	7600
A	7.02	14	0.8	4	2500

concentrations of Fe and Mn were observed in the coolant particulate. The tendency of increasing Ni composition is obvious as the plant operation time increases. The specific activities at start-up were usually higher than that at steady state except during cycle 3 of Doel 3. That may indicate that the water chemistry during the start-up increases dissolution rate of crud from the fuel rod, and/or flow conditions during start-up cause a temporary increase in the erosion rate of crud from the fuel. In general, ^{60}Co specific activity increases as the plant operation time increases.

The Korea Electric Power Research Institute (KEPRI) has investigated the composition of steam generator crud and coolant particulate from Kori-1.[22] The results are given in Table 3-4. KEPRI results also show a high concentration of Fe in the coolant particulate like the results from Doel. However, it reveals somewhat different characteristics. Firstly, it looks unusual that considerable amount of chromium was found in the coolant particulate. Generally, chromium is considered to remain in the oxide film, but the coolant particulate from Kori 1 contain about 10 % of chromium. It may be explained by the increased contribution of erosion from the surface of out-core components due to the increased thickness of oxide film on the surface. Secondly, the high concentration of nickel in the coolant particulate should be noted. As noted earlier for Doel, the nickel concentration in the coolant particulate is likely to be increased with the operation history of the plant. Finally, the Ni/Fe ratio was generally higher than that found in the coolant particulate from Doel and that found in the steam generator crud from Westinghouse plants A to H. It was rather close to the ratio found in the fuel deposits from the WEP and NOK cores.

Balakrishnan and Allison have implemented some in-reactor loop experiments on corrosion product transport and water chemistry.[7] Radiochemical analysis results of crud and the composition of corrosion products in the coolant at normal chemistry condition are shown in Table 3-5. From the radiochemical results, the following interesting points can be noted:

- Relatively high specific activity of coolant particulate crud compared to that of dissolved species in the coolant

Table 3-3

Composition and Specific Activity of Coolant Particulate from Doel 3&4

• Concentration and composition

		Concentration in Coolant, $\mu g/dm^3$ (% Composition, w.r.t. Total Oxides)				
Plant	Cycle	Fe	Ni	Co	Mn	Ni/Fe Ratio
Doel 3	1	1.40 (71)	0.10 (4.8)	0.002 (0.12)	0.08 (3.4)	0.07
	2	0.41 (57)	0.06 (8.3)	0.001 (0.12)	0.03 (4.0)	0.15
	3	1.02 (52)	0.32 (16.0)	0.002 (0.11)	0.04 (2.4)	0.31
Doel 4	1	0.23 (59)	0.04 (10.0)	0.001 (0.25)	0.01 (2.5)	0.17
	2	1.10 (55)	0.29 (14.5)	0.002 (0.08)	0.05 (2.5)	0.26

• Specific activity of ^{58}Co and ^{60}Co

Plant	State	Cycle 1		Cycle 2		Cycle 3		Cycle 4	
		^{60}Co	^{58}Co	^{60}Co	^{58}Co	^{60}Co	^{58}Co	^{60}Co	^{58}Co
Doel 3	Start-up					550 (15)	15 (0.4)	670 (18)	15 (0.4)
	Steady	59 (1.6)	15 (0.4)	100 (2.7)	15 (0.4)	270 (7.3)	44 (1.2)		
	Shutdown	1260 (34)	11 (0.3)	520 (14)	11 (0.3)	150 (4)	4 (0.1)		
Doel 4	Start-up			410 (11)	15 (0.4)				
	Steady	22 (0.6)	15 (0.4)	140 (3.8)	11 (0.3)				
	Shutdown			1260 (34)	66 (1.8)				

Note) Specific activity : GBq (Ci) $^{60}Co/gm\ ^{59}Co$
GBq (Ci) $^{58}Co/gm\ ^{58}Ni$

Table 3-4

Composition of Crud from Kori 1[22)]

(Unit : wt%)

Element	S/G Cold Leg Chamber (Cycle 10)	S/G Tube	Particulate in Coolant	
			Cycle 10 (Refueling)	Cycle 12 (Steady State)
Fe	32.8	26.8	66.3	60.3
Ni	45.7	47.2	22.5	30.4
Cr	21.3	24.7	10.5	8.4
Co	0.5	0.56	0.1	0.17
Ni/Fe	1.85	1.76	0.34	0.50

Note) Only metal components are included when calculating wt%.

- Nearly the same specific activity of dissolved species as found in pipe section deposits
- Great effect of high temperature filtration on the specific activity
- Same $^{60}Co/^{58}Co$ ratio between fuel deposit and coolant particulate
- Remarkable decrease in the specific activities of ^{58}Co and ^{59}Fe with filtration

The composition of corrosion products present in the coolant from the in-reactor loop experiments shows characteristics typical of the release mechanism from the oxide film. If the release mechanism is governed by the ionic diffusion through the

Table 3-5

Crud Analysis Data from Some In-Reactor Loop Experiments[7)]

• Radiochemical Analysis Results of Crud (Specific Activity)

		Fuel Deposit*	Without Filtration			With Filtration		
			Pipe Section Deposit	Particulate Crud	Dissolved Species	Pipe Section Deposit	Particulate Crud	Dissolved Species
Specific Activity	^{60}Co	72,000	5,440	17,400	5,180	3,260	15,500	
	^{58}Co	960		48	209*		93	
	^{59}Fe	173		30	1.1*		7.4	
$^{60}Co/^{58}Co$		3.0		3.1	5.5		8.6	12

Note) Chemistry condition : pH 10 to 10.5 with LiOH: H_2: 3 to 7 cm^3(STP)/kg
Specific Activity : GBq ^{60}Co/kg Co; GBq ^{58}Co/kg Ni; GBq ^{59}Fe/kg Fe
* The values are estimated from the data given in Ref. 7.

• Composition of Corrosion Products in the Coolant (Without Filtration)

	Corrosion Product Concentration, μg/kg Coolant (Weight Percent*)	
	Insoluble	Soluble
Fe	2.75 (45.6)	3.0 (85.5)
Ni	2.64 (43.8)	0.23 (6.6)
Cr	0.59 (9.9)	0.09 (2.6)
Co	0.04 (0.7)	0.06 (1.7)
Mn	-	0.13 (3.7)

* Weight percent was evaluated for the above five elements to see the relative contribution of each element.

pores within oxide layer, the diffusion coefficient for each element may be different. It may also cause the preferential release of the elements. A relatively high concentration of Fe and Co in the dissolved species in the coolant suggests that Fe and Co are easily released from the oxide film compared to the other elements.

Alloy weight changes were measured for stainless steel 304L, Inconel-600 and Zircaloy-4 after exposing coupons to coolant up and downstream from the filter.[18] The results for the untreated coupons are summarized in Table 3-6. Continuous increase in the weights of stainless steel and Zircaloy-4 was observed at the EMF inlet during the test period. It suggests the deposition rate of crud into oxide film is higher than the release rate from the oxide film in the solution saturated with corrosion products. On the contrary, weights of Inconel-600 coupons decreased with the exposed time. Therefore, it is possible to conclude that the release rate from the oxide formed on the surface of Inconel-600 is much higher than that from the oxide formed on the surface of stainless steel. There was no increase in the weight of stainless steel after 75 day's exposure at the EMF outlet. It seems to have reached an equilibrium state between deposition rate and release rate.

From the data given in Table 3-6, it is apparent that constituents of the metal are not released in proportion to their concentration in the base metal. Table 3-7 shows the percent enrichment or depletion of elements released from Inconel-600 and stainless steel 304.[16] For example, the corrosion products released into the coolant from the oxide film formed on the surface of stainless steel will be enriched in cobalt by about 70%. The composition of the corrosion products released from the Inconel-600 will show the enrichment of cobalt by about 140% while the enrichment for iron is over 300%.

Table 3-6

Alloy Weight Changes of Untreated Coupons
Exposed to Coolant Up and Downstream from the Filter

Test Alloy	EMF Inlet		EMF Outlet	
	75 Day	148 Day	75 Day	148 Day
Stainless Steel 304L	+238	+659	+262	+262
Inconel-600	-198	-2151	-95	-2119
Zircaloy-4	+167	+206	+294	+135

Note) Weight changes expressed as $\mu g/cm^2$.

Table 3-7

Percent Enrichment or Depletion of Elements
Released from Inconel-600 and Stainless Steel 304

	Element	Base Metal %	Released %	Released Percent (Enrichment or Depletion)
Inconel-600[a]	Ni	77	57	-25 %
	Cr	16	13	-19 %
	Fe	7	30	329 %
	Co	~0.08	0.19	137 %
Stainless Steel[b]	Co	0.069	0.115	67 %
	Mn	1.05	0.905	-18 %

a. Inconel at 500 °F at pH 10 to 10.5 at 25 °C with LiOH
b. Stainless steel 304 at 600 °F with 1050 ppm boron as boric acid and 1.6 ppm lithium as lithium hydroxide

3-1-2 Release Mechanism from Corroded Surfaces

From the above results, it is possible to infer some characteristics related to the release mechanism from corroded surfaces. One important feature might be the preferential release of metal ions shown in Table 3-7. The Ni/Fe ratio of crud and that of base metal indicates the preferential release mechanism of metal ions onto the coolant from the oxide film formed on the surface of base metal. SEM-EDAX analysis results which show the diffusion of Fe towards the surface of film also support this mechanism. The low chromium content in the fuel deposit from WEP and NOK cores and the coolant particulate from Kori-1 imply the low release rate of chromium from the oxide film. It's not easy to define the tendency of cobalt release mechanism from the cobalt composition data obtained by the analysis of crud. However, the enrichment data of cobalt in the coolant shows cobalt to be released into the coolant very easily.

Clearly, there is no similarity in the crud compositions between the coolant particulate and the deposits on the out-core surfaces. It may imply that release mechanism between the coolant and the corrosion film is controlled by ionic diffusion from the surface of oxides to the coolant except for crud burst conditions.

The Ni concentration in the coolant shows a tendency to increase with the plant operation time. That is because the relative concentration of Ni in the corrosion film probably increases with time due to the preferential release of Fe and Co into the coolant. Also, some evidence may suggest the high release rates of Ni and Cr during high power operation. It is not clear what the relationship between the release rates of Ni and Cr and the power level of core might be. However, the increase of deposition of Ni and Cr from the coolant onto the fuel rod surface at high power can be a driving force inducing the release of Ni and Cr into the coolant from corroded surfaces.

Alloy weight changes during exposure to the coolant[18] shows a constant decrease in the weight of Inconel-600 coupons, whereas some increases are found in the weight of stainless steel coupons. It indicates that the release rate from the oxides

formed on the surface of Inconel-600 is much higher than that from the oxides formed on the surface of stainless steel. This can be inferred from the data for the cobalt release rates reported in Ref. 16.

3-1-3 Deposition of Corrosion Products onto the Fuel Rod Surface

The composition of fuel deposits reveal no strong evidence to show the deposition mechanism onto the fuel. However, if we suppose the deposition mechanism is governed by the mechanism of crystallization from the soluble species in the coolant, it must be the elemental preferential process, which is contrary to the release mechanism of elements from the oxides formed on the out-core surfaces. Low composition of cobalt in the fuel deposit from WEP and NOK cores indicates the possibility of low deposition rate of cobalt compared to that of Ni or Cr. Quantitative relationships can not be shown from the above investigated results.

It cab be inferred that heat flux may have an important role to enhance the deposition rate of Co and Cr from the data of NOK cycle 3 cores. The contributions of cobalt and chromium have increased more than two times at high power fuel bundles.

3-1-4 Release Mechanism of Activated Products from the Fuel Rod Surface

Specific activity of particulate crud in the coolant was relatively high compared to the specific activity of dissolved species in the coolant. It may imply that most of activated corrosion products are released in the form of particulate from the fuel rod surface into the coolant by erosion. And the same ratio of ^{60}Co to ^{58}Co between fuel deposits and the coolant particulate can be interpreted to support this release mechanism.

It can be noted from the data of Doel 3 & 4 that the release of activated products

from the fuel rod surface may depend on the chemistry condition of the coolant. The particulate data show the highest specific activity at start-up and the lowest at shutdown. This means that startup chemistry conditions increase the release rate of cobalt from the in-core components, and shutdown conditions increase the release rate of cobalt from the out-core components.

3-1-5 Deposition Mechanism of Activated Products onto Out-core Surfaces

The specific activities of dissolved species were nearly the same as that of deposits found in the pipe section. Contrary to the release mechanism from the fuel rod into the coolant, this may imply that deposition of activated corrosion product from the coolant onto the out-core surfaces must be controlled by the crystallization process of dissolved species. However, particulate deposition is also suspected from the high specific activity of pipe section deposits.

The specific activity of ^{60}Co in the coolant particulate was quite different from that of the dissolved species. It may indicate that exchange reaction of cobalt between cobalt ions incorporated into the crystal structure and the dissolved cobalt ions is very slow. The exchange reaction can be modeled by assuming some deposited metal ions are replaced by particulates in the coolant.

3-2 Release Model of Cobalt Source onto the Coolant

In order to evaluate the input of cobalt into the primary system, the release model of corrosion products from the oxide formed on the surface of structural materials into the coolant should be defined. In this report, the following premises will be assumed to get an analytical solution for the released quantity.

- The corrosion rates of base metals are constant; the corrosion mechanism is described by linear kinetics.

- After the equilibrium state is reached between dissolved species and particulate in the coolant, the exchange rate of cobalt between them is negligible.

- Cobalt from the oxide films that form on the surface of structural materials is released as cobalt ions into the coolant. As discussed above, the release mechanism will be considered to be a preferential ionic release mechanism. Cobalt produced by wear is released as particles which are assumed to subject to oxidation in the coolant immediately and become particulate corrosion products. However, even the cobalt input from the wear of Stellite-6 will be treated as ionic release for analytical convenience.

- The release rate of metal ions from the oxide film is proportional to the total weight of oxide that forms on the surfaces of base metals. It looks somewhat illogical, because the release rate per oxide thickness by diffusion process of ions will decrease as the oxide thickness increases due to the increased interactions between ions in the pore. However, some authors show this simple model provides good agreement with the experimental results.[3,4,7]

- The relative cobalt concentration in the dissolved species is higher by the enrichment factor than that in the oxide film. This can be inferred from the difference of cobalt concentration between dissolved species and oxide film.

- Cobalt released from the surface of Stellite-6 by wear and corrosion will be released directly into the coolant.

3-2-1 Release Rate of Cobalt into the Coolant

Since the corrosion rate of the base metal was assumed to be constant, the total quantity of base metal to be incorporated into the oxide film at time t can be expressed as the following simple equation.

$$Q(t) = k_c \cdot t \qquad \text{----------} \quad (3)$$

where $Q(t)$: weight of base metal incorporated into the oxide film, g/m^2

k_c : corrosion rate constant, $g/m^2 \cdot s$

The release rate of metal ions from oxides by ionic dissolution was assumed to be proportional to the total weight of film oxides forming on the surface. Therefore, the release rate of metal components from the oxide film into the coolant can be expressed as follows,

$$R(t) = r_o \, W_o(t) \qquad \text{----------} \quad (4)$$

where $R(t)$: release rate of metal components from the oxide film formed on the metal surface into the coolant, $g/m^2 \cdot s$

$W_o(t)$: weight of metal components contained in the oxide film formed on the metal surface at time t, g/m^2

r_o : oxide film release rate constant, s^{-1}

However, cobalt will be preferentially released from the oxide film into the coolant. Therefore, the weight percent of cobalt in the dissolved species will show a somewhat higher value compared to that in the oxide film formed on the metal surfaces, which can be explained with the released enrichment factor given in Ref. 16. The enrichment factor in Ref. 16 can be defined as follows under the assumption of no metal removal from the coolant.

$$(1+e)\ f_{Co} = \frac{R'_{Co}(t)}{R'(t)} \qquad \text{---------- (5)}$$

where e : cobalt enrichment factor into the released ions

f_{Co} : weight fraction of ^{59}Co in the base metal

$R'_{Co}(t)$: total weight of cobalt released as the dissolved species into the coolant at time t, g/m^2

$R'(t)$: total weight of metal components released as the dissolved species into the coolant at time t, g/m^2

The total weight of metal components released as the dissolved species into the coolant, $R'(t)$ can be calculated from the total weight of metal components incorporated into the oxide film and that of the remaining oxide film by assuming no re-deposition from the coolant. This assumption may represent the short-term experimental condition, or a system from which the released corrosion products are removed constantly.

$$R'(t) = Q(t) - W_o(t) \qquad \text{---------- (6)}$$

Since $R'(t)$ can be obtained by integrating $R(t)$ from 0 to t, $R'(t)$ can be expressed as the first-order differential equation from Eq. (4) and Eq. (6).

$$\begin{aligned} R(t) = \frac{dR'(t)}{dt} &= r_o\ W_o(t) \\ &= r_o\ Q(t) - r_o\ R'(t) \\ &= r_o\ k_c\ t - r_o\ R'(t) \qquad \text{---------- (7)} \end{aligned}$$

And the solution to Eq. (7) gives

$$R'(t) = k_c\ t - \frac{k_c}{r_o}\ (1 - e^{-r_o\ t}) \qquad \text{---------- (8)}$$

From Eqs. (5) and (8), the release rate of cobalt from the oxide film into the

coolant can be expressed as:

$$R'_{Co}(t) = f_{Co}\, k_c\, (1+e)\, [\, t - \frac{1}{r_o}\, (1 - e^{-r_o t})\,] \qquad \text{----- (9)}$$

Again, the release rate of metal components and cobalt from the base metal into the coolant can be obtained by differentiating $R'(t)$ and $R'_{Co}(t)$. Therefore, $R(t)$ and $R_{Co}(t)$ have the following simple expressions.

$$R(t) = k_c\, (1 - e^{-r_o t}) \qquad \text{---------- (10)}$$

$$R_{Co}(t) = f_{Co}\, k_c\, (1+e)\, (1 - e^{-r_o t}) \qquad \text{---------- (11)}$$

In the above equation, the cobalt enrichment factor into the released ions for the major materials used in PWRs will be assumed to be as follows based on Ref. 16.

Inconel-600	137 %
Stainless steel	67 %
Stellite-6	assume no enrichment

3-2-2 Evaluation of Release Rate Constant

Now we have to determine the release rate constant in order to evaluate the corrosion input to the coolant from the total weight of base metal incorporated into the oxide film, $Q(t)$, and the total weight of metal components released as the dissolved species into the coolant, $R'(t)$. From Eq. (3) and Eq. (8), it is possible to derive the released ratio of metal components incorporated into the oxide film.

$$\gamma = \frac{R'(t)}{Q(t)} = 1 - \frac{1}{r_o\, t}(1 - e^{-r_o t}) \qquad \text{---------- (12)}$$

where γ is the release ratio of oxide film as dissolved species into the coolant

It is also possible to determine the value of γ from some experimental results. In this report, we used the data provided in Ref. 16 in order to evaluate the release rate constant. Table 3-8 shows the release ratios which are obtained by dividing the corrosion rates with the release rates given in Ref. 16.

By applying the data for the test time and release ratio from the Table 3-8 into Eq. (12), it is possible to determine the release rate constant. Since the corrosion rate and the release rate given in the table show large differences depending on the experimental conditions, we used the data for annealed materials. However, the data for stainless steel shows a big deviation, therefore, it is recommended to re-evaluate it by using same methodology whenever the data are available. For Inconel-600, there are three data for the annealed specimens, and they showed quite good agreement. The release rate constants evaluated for stainless steel and Inconel-600 are

$$r_o = 4.16\times10^{-7} \pm 4.94\times10^{-7} \quad s^{-1} \qquad \text{for stainless steel}$$

$$r_o = 5.56\times10^{-8} \pm 7.17\times10^{-9} \quad s^{-1} \qquad \text{for Inconel-600}$$

Deposition from the coolant into the oxides was not considered in the above process of evaluating r_o. However, if the experiments were conducted in a closed autoclave, the release rate constant might be underestimated.

Table 3-8

Release Ratios of Metal Ions from the Oxides into the Coolant

Material	Temp. (℃)	Alkalinity	Test Time (Months)	Corrosion Rate (μm/yr)	Release Rate (μm/yr)	Release Ratio (γ)	Comments
304 S/S	315	10^{-4}M LiOH, 1050 ppm B	2	2.3	1.3	0.565	Annealed
	315	10^{-4}M LiOH, 1550 ppm B	9.2	0.6	0.3	0.5	Annealed
	315	10^{-4}M KOH, 1550 ppm B	9.2	0.5	0.3	0.6	Cold Worked
Inconel-600	315	10^{-4}M LiOH, 1050 ppm B	2	3.4	0.5	0.147	Annealed
	315	10^{-4}M KOH, 1550 ppm B	9.2	2.2	0.9	0.409	Annealed
	315	10^{-4}M KOH, 1500 ppm B	3	4.6	1.5	0.326	Grit Blasted
	315	10^{-4}M KOH, 1500 ppm B	4	2.1	0.5	0.238	Annealed
	315	10^{-4}M KOH, 1550 ppm B	9.2	2.2	0.8	0.364	

4. IN-CORE ACTIVATION OF COBALT

4-1 In-Core Deposition and Release Mechanism

In order to evaluate the amount of crud deposited on the fuel rod, the following conditions will be assumed based on previous findings:

- All corrosion species, including wear products, begin as dissolved ions which agglomerate into progressively larger particles under the influence of both Brownian motion and shear flow.

- Particles are transported to the wall by fluid eddies, and stick to the wall by their inertia. In other words, deposition from the coolant onto the in-core fuel rod surface is controlled by particulate adhesion process.

- There is no interaction between particles in the coolant, so every particle deposits independently onto the surface of the fuel. Therefore, the deposition rate of particulate is proportional to the concentration of particulate in the coolant. Some experimental results appear to support this assumption in the low concentration range, and the particulate concentration in the primary coolant system is thought be low enough to apply this assumption in the normal operating condition for calculating the weight of deposits on the fuel rod surface.

- Deposition is a reversible process, i.e., the amount of deposit on the fuel rod might decrease to a steady lower value if the environment changes to one less favourable for deposition. The release rate of deposit from the fuel rod is assumed to be proportional to the thickness of the deposits.

- The deposits are released as particulate by erosion from the fuel rod into the coolant. This can be logically inferred from the experimental results which show a good resemblance between fuel deposits and particulate.

Deposits on the fuel consists of two components, i.e., the adherent deposit layer and the loose deposit layer. Measurement of ^{60}Co in the coolant during start-up suggests the incorporation reaction between two layers may be reversible. If two layers exist in the fuel rod deposits, the total weight of deposits on the fuel can be expressed as follows:

$$W_F = W_a + W_l \quad \text{---------- (13)}$$

where W_F : total weight of deposits on the fuel rod, g/m^2

W_a : weight of the adherent deposit on the fuel rod, g/m^2

W_l : weight of the loose deposit on the fuel rod, g/m^2

Then, the process of crud build-up on the fuel rod can be described with several simple differential equations.

$$\frac{dW_l}{dt} = k_f C_p - (r_f - k_l) W_l + k_a W_a \quad \text{---------- (14)}$$

$$\frac{dW_a}{dt} = k_l W_l - k_a W_a \quad \text{---------- (15)}$$

where C_p : weight concentration of metal components contained in the suspended particulate in the primary coolant, g/m^3

r_f : erosion rate constant of deposit from the fuel rod into the coolant, s^{-1}

k_f : deposition rate constant from the particulate in the coolant onto the fuel rod surface, m/s

k_a : incorporation rate constant from the adherent layer to the loose layer, s^{-1}

k_l : incorporation rate constant from the loose layer to the adherent layer, s^{-1}

The equations can be solved analytically for W_l and W_a by assuming a constant ratio between W_l and W_a, i.e. $W_a = f \cdot W_l$. The analytical solutions can be

expressed as follows:

$$W_l = \frac{k_f C_p}{K_1} (1 - e^{-K_1 t}) \quad \text{---------- (16)}$$

$$W_a = \frac{K_2}{k_a} - \frac{K_2}{k_a - K_1} e^{-K_1 t} + K_2\left(\frac{1}{k_a - K_1} - \frac{1}{k_a}\right) e^{-k_a t} \quad (17)$$

where $K_1 = r_f + k_l - f \cdot k_a$, and

$$K_2 = \frac{k_f k_l C_p}{K_1}$$

In order to use the above equations, we need the information on the characteristics of deposits formed on the fuel rod in order to determine the rate constants and f value. However, we only have limited information. Therefore, we cannot use them for the practical purpose at this moment, even though it is possible to solve the equation for some radioactive nuclides and obtain rate constants by assuming the f value. However, it is more practicable to assume a one layer structure for fuel rod deposits. Balakrishnan and Allison have calculated the rate constants for this simple case.[7] In this report, we followed their approach for the evaluation of the rate constants except the slight change for the activation equation.

By assuming a release rate constant that is independent of deposit thickness, the weight of deposits on the fuel can be given by an equation similar in form to Eq. (16).

$$W_F = \frac{k_f C_p}{r_f} (1 - e^{-r_f t}) \quad \text{---------- (18)}$$

Since the release of deposits from the fuel rod into the coolant is assumed to be caused by erosion, it is reasonable to suppose the same composition between deposits and the released particles. In this case, the rate constant for each element in the deposit is the same as that for the deposit. Thus, r_f can be used to evaluate the release rate of cobalt from fuel rod to coolant.

4-2 Activation of Crud in the Core

A nuclide deposited on the fuel rod can absorb a neutron, transforming it into a radioactive nuclide. The buildup rate of a given radioactive nuclide, a, on the fuel rod is given by the following expression.

$$\frac{dn_a}{dt} = W_F\, n\, (\sigma_{th}\, \psi_{th} + \sigma_{ep}\, \psi_{ep}) - (\lambda + r_f) n_a + k_f\, n_{pa}\, C_p \qquad (19)$$

where n_a : number of a given radioactive nuclei present in the fuel deposits

n : number of parent target nuclei per gram deposits on the fuel as metal elements, g^{-1}

n_{pa} : number of a given radioactive nuclei per gram particulate as metal elements deposited from the coolant onto the fuel

λ : radioactive decay constant of the radioactive nuclide, s^{-1}

σ : activation cross section of the parent nuclide, m^2

ψ : neutron flux for thermal neutron or epithermal neutron, $m^{-2} \cdot s^{-1}$

In Eq. (19), n can be considered as a constant because n_a, which represents the number of parent nuclei transformed into radioactive nuclei by absorbing a neutron, is much smaller than n. In this equation, n_{pa} must be a time-dependent variable. So, it is impossible to solve the equation without knowing the relationship between n_a and n_{pa}. However, particulates in the coolant entering the core carry small quantities of radioactive nuclei compared to that present in the fuel deposit. Therefore, no contribution of the newly deposited crud to the buildup of the nuclide is assumed for the evaluation of the rate constants.

By substituting W_F in Eq. (19) with Eq. (18), then integrating with time, n_a can be obtained as follows:

$$n_a = \frac{k_f\, C_p\, n}{\lambda} \left[\frac{\lambda (\sigma_{th} \psi_{th} + \sigma_{ep} \psi_{ep})}{r_f (\lambda + r_f)} \right.$$

$$- \frac{\sigma_{th}\psi_{th} + \sigma_{ep}\psi_{ep}}{r_f} e^{-r_f t}$$

$$+ \frac{\sigma_{th}\psi_{th} + \sigma_{ep}\psi_{ep}}{\lambda + r_f} e^{-(\lambda + r_f) t}] \quad \text{---------- (20)}$$

The activity accumulated on the fuel due to the radionuclide produced is λn_a. Therefore, the specific activity(S_A) in units of kBq/kg can be obtained as follows:

$$S_A = \frac{\lambda n_a}{W_F} = \frac{n}{(1 - e^{-r_f t})}$$

$$\times [\frac{\lambda(\sigma_{th}\psi_{th} + \sigma_{ep}\psi_{ep})}{\lambda + r_f}$$

$$- (\sigma_{th}\psi_{th} + \sigma_{ep}\psi_{ep}) e^{-r_f t}$$

$$+ \frac{r_f(\sigma_{th}\psi_{th} + \sigma_{ep}\psi_{ep})}{\lambda + r_f} e^{-(\lambda + r_f) t}] \quad \text{---- (21)}$$

Here, it should be noted that the specific activity means the radioactivity of a certain radionuclide in unit of kBq per kg of deposits as metal components. In this report, mathematical analysis is based on only the metal components which are constituents of the metal oxides.

4-3 Evaluation of Rate Constants

Now, it's possible to evaluate the erosion rate constant, r_f, in Eq. (21) and the deposition rate constant, k_f, in Eq. (18) by using the measured data from the WEP core and the in-reactor loop experimental results of Balakrishnan and Allison.[6,7,10] Table 4-1 shows the value for each parameter used to evaluate the rate constants.

The values of r_f obtained by using the data given in the Table 4-1 are 3.01×10^{-6} s^{-1} for the WEP cycle 1, and 1.11×10^{-6} s^{-1} for the in-reactor loop experiments. The two results show good agreement, even though some data of the WEP cycle 1 are assumed from the calculated values. The data from the NOK cycle 1 are not used here, because the crud thickness on the fuel looks exceptionally high.[10] The value of k_f obtained from the in-reactor loop experiment data is 1.0×10^{-6} m/s. The concentration of particulate in the coolant for WEP cycle 1 was not given in the reference, so we can't evaluate k_f from the data of WEP cycle 1. It is very important to use measured values when evaluating k_f, because k_f is inversely proportional to C_p. Errors in the value of C_p will cause errors in k_f.

Another possible problem may raise if we rely on the experimental data. The problem is the possibility of underestimating the thickness of deposits on the fuel. As noted in the previous chapter, particulates in the coolant seems to adhere more on the surface of high power fuel rods than on low power fuel rods. So, if we use the value of k_f evaluated from the experimental data which are obtained in the low power environment compared to the PWR core condition, then the thickness of fuel deposits estimated by using the value of k_f may be lower than the real thickness. Therefore, we assumed the concentration of particulate in the coolant as the average value found during the first cycle of Doel 3 and 4, and evaluated k_f again. The value of k_f then is in the range of $9.7\times10^{-5}\sim6.5\times10^{-3}$ m/s, which is much higher than the value evaluated from the in-reactor loop experiment results.

In this report, the geometric average of the low limit value and the high limit value

obtained from WEP cycle 1 will be adopted as the deposition rate constant from the coolant onto the fuel rod surface. In the same way, the geometric average of r_f for WEP cycle 1 and the in-reactor loop experiment will be chosen as the release rate constant from the fuel rod surface into the coolant for the evaluation of ^{60}Co buildup in the primary coolant system of PWRs. The rate constants so calculated are

$$r_f = 1.83 \times 10^{-6} \quad s^{-1}$$

$$k_f = 7.94 \times 10^{-4} \quad m/s$$

The rate constants may be re-estimated by using the above method when new data are available.

Table 4-1

The Value for Each Parameter Used to Evaluate the Rate Constants

Source	W_F[a] (g/m^2)	S_A (kBq/kg)	n[b] (g^{-1})	σ_{th} (m^2)	ψ_{th}[c] ($m^{-2}s^{-1}$)	σ_{ep}[d] (m^2)	λ (s^{-1})	t[e] (s)	C_p[f] (g/m^3)
WEP Cycle 1	0.03~2.02	1.18×10^{8}	5.80×10^{18}	3.72×10^{-27}	2.1×10^{18}	3.28×10^{-27}	4.18×10^{-9}	2.63×10^{7}	9.32×10^{-4}
Loop Experiments (Without Filtration)	5.52×10^{-2}	2.6×10^{8}	3.70×10^{19}		5×10^{17}	-		1.97×10^{7}	6.09×10^{-3}

a. The value of W_F from WEP cycle 1 was re-evaluated to include metal components(Fe, Ni, Cr, Mn, and Co) only.

b. $$n = \frac{\text{weight fraction of Co}}{\text{M}} N_A$$
$$= \frac{\text{weight fraction of Co}}{59} \times 6.024\times10^{23}$$

c. ψ_{th} for WEP cycle 1 was evaluated from the residence time of ^{51}Cr from the following equation.

$$\psi_{th} = \frac{W_A S_A}{36.12\, a_i\, (\sigma_{th}+\sigma_{ep})(1-e^{-\lambda t})}$$

d. σ_{ep} has been adjusted by the ratio of epithermal-to-thermal neutrons in Ref. 10.

e. Irradiation time, t was assumed as 10 months for WEP cycle 1.

f. The particulate concentration in the coolant from the loop experiments was re-adjusted to include the metal components only(excluding Zr) from the out-core components. The average value was used as the particulate concentration for WEP cycle 1.

5. ANALYSIS OF OUT-CORE DEPOSITION

5-1 Base Material

Cobalt input into the primary coolant system is basically determined by the amount of corrosion products produced from the structural materials, and the amount of corrosion products released into the coolant. The corrosion kinetics and the release kinetics can be affected by several factors. The base material is one of the most fundamental factors that must be considered.

Several differences in the corrosion rate and the release rate between stainless steel and Inconel-600 have been reported. The corrosion rate of Inconel-600 is much higher than that of stainless steel.[1)] Unlike the corrosion kinetics, it is not easy to compare the release rates of stainless steel and Inconel-600 because the release ratio shows a considerable variation depending on the experiments. However, the release rate of metal ions from the oxides which form on the surface of Inconel-600 is assumed to be a bit lower than that from the oxides which form on the surface of stainless steel as shown in Chapter 2. High dissolution rate of Fe found in the experiments may also support this assumption.

However, micrographs of oxide film formed on the surface of Inconel-600 shows that oxide film has the substantially less structured layer than that formed on stainless steel. Also, the result of weight change measurements during the exposure of test coupons up and down-stream of EMF filters shows that Inconel-600 loses weight continuously, while stainless steel gains weight during exposure. From these interesting findings, it is possible to conclude that the deposition rate from the coolant onto the oxide film formed on the surface of stainless steel may be much higher than that from the coolant onto the oxide film formed on the surface of Inconel-600.

From the Lister's analytical results, it is also possible to infer the deposition kinetics onto the surfaces of structural materials. Lister expressed the deposition

function, $\eta(t)$, in terms of transport resistances, assuming double layers of oxide films form on the surfaces of structural materials.[12,23)]

$$\eta(t) = \frac{1}{DIFF_i + CRYST_i} + \frac{1}{CRYST_o} \quad \text{---------- (22)}$$

where $DIFF_i$ is the differential resistance within the inner oxide layer and $CRYST_i$ and $CRYST_o$ are the resistances associated with the crystallization of the inner and outer layers. So, the activation of the fine grained inner layer is governed by two transport resistances in series: diffusion down the pores of the film to the metal/oxide interface($DIFF_i$) followed by crystallization($CRYST_i$). However, the activation of the outer layer is governed solely by a crystallization resistance ($CRYST_o$). The resistances for stainless steel and Inconel-600 are given as follows.[12,23)]

For stainless steel,

$$DIFF_i = \frac{m(t)}{2\rho D\varphi(1-\varphi)} \quad \text{---------- (23)}$$

$$CRYST_i = \frac{C_{si}}{0.35\,\frac{dm(t)}{dt}} \quad \text{---------- (24)}$$

$$CRYST_o = \frac{C_{so}}{0.35\,\frac{dm(t)}{dt}} \quad \text{---------- (25)}$$

where $m(t)$: amount of oxide formed on the surface, g/m^2

ρ : oxide density, g/m^3

φ : oxide layer porosity

D : diffusion coefficient of radioactive ions in coolant, m^2/s

C_{si}, C_{so} : solubilities of inner and outer layer oxides, g/m^3

For Inconel-600 tubing,

$$DIFF_i = \frac{m(t)}{\rho D \varphi (1-\varphi)} \qquad \text{---------- (26)}$$

$$CRYST_i = \frac{C_{si}}{0.7 \frac{dm(t)}{dt}} \qquad \text{---------- (27)}$$

$$CRYST_o = \frac{C_{so}}{0.18\ d\ u \frac{dC_{so}}{dT} \frac{dT}{dx}} \qquad \text{---------- (28)}$$

where d : tube diameter, m

u : velocity of coolant in the tube, m/s

x : distance from tube inlet, m

T : temperature

However, if we can assume that incorporation into the outer layer is dominant compared to that into the inner layer, then the activation rate becomes to be governed by the incorporation rate into the outer layer. Then, the activity deposition rate per unit surface area from coolant into the oxide film will have the following expression.

$$A_d(t) = C_b(t) \cdot \eta(t) \qquad \text{---------- (29)}$$

where $A_d(t)$: activity deposition rate per unit surface area, Ci/m^2

$C_b(t)$: concentration of radioactivity in the bulk stream, Ci/m^3

From Eq. (29), it is possible to conclude that the activity deposition rate is proportional to the bulk concentration, if $\eta(t)$ is constant. It looks reasonable to express the $\eta(t)$ for Inconel-600 tubing as a constant value for the typical steam generator of PWRs.[23] Also, $\eta(t)$ becomes constant for stainless steel, because the corrosion rate of stainless steel was assumed to be constant in this report.

It may be necessary to compare the deposition rates of stainless steel and Inconel

by using Lister's model. Lister has evaluated the value of $\eta(t)$ for stainless steel and Inconel-600 tubing as follows:[23]

$$\eta(t) = 6.08\times10^{-3} \quad cm/s \quad \text{for Inconel tube}$$

$$\eta(t) = \frac{1.57\times10^{-2}}{2.09\times10^{-2}\,t + 1} \quad \text{for stainless steel}$$

From the above equations, we can presume the deposition rate into the oxide film formed on the surface of stainless steel will decrease quite rapidly with time. For example, the deposition function for stainless steel will be the same as that for Inconel in 80 hour (about 3.4 days), and it will be reduced to one-tenth of that for Inconel tube in 50 days. It is unlikely that deposition into the inner layer may become more dominant with the lapse of time. Therefore, some experimental results, which show that the deposition rate into the oxide film formed on the surface of stainless steel is much higher than that into the oxide film formed on the surface of Inconel-600, may not be explained by the above deposition kinetics.

In order to reflect the difference of deposition rate caused by the different base metal, we have evaluated the deposition rate constants for stainless steel and Inconel-600 as follows. It seems to be clear that the deposition mechanism into the oxide film is governed by the crystallization of the dissolved species in the coolant into the oxide film judging from the similar radiochemical composition between dissolved species and oxide film even though there is another possibility for that coincidence.[7] If we neglect the deposition mechanism into the inner layer, it is possible to assume that the deposition rate is proportional to the concentration of dissolved species in the coolant. From the mass balance across the oxide film, the equation, which describes the weight of oxide film formed on the surface at time t, can be obtained. Again, it is possible to derive the equation for the activity of ^{60}Co, and compare it with the result calculated from a logarithmic expression for the accumulation of activity appeared in some references. By assuming the long-term pseudo-steady state, then, the deposition rate constants for stainless steel and Inconel-600 will be evaluated.

5-2 Water Chemistry

Some efforts have been concentrated on the control of water chemistry to reduce occupational radiation exposure of workers. It is well known that it is possible to minimize the amount of fuel deposit in a certain pH band, thereby to minimize the production of activated corrosion products. Some experimental results for particulate corrosion products in the coolant, which show the effect of pH are illustrated in Table 5-1. From the Table 5-1, the following effects of water chemistry on crud transport can be noted.

- Reducing the coolant pH from the range of 10 to 10.5 to below 9.5 caused an appreciable increase in the crud concentration in the water. But increasing the pH above did not.

- The amount of activity being transported by the water increased, due not only to the higher concentration but also to a greater amount of active nuclides per unit weight of crud. The increased activity indicates that some of the crud making up the higher concentrration had come from deposits on the fuel. Also, it is possible to say that the residence time in the core may increase with lowering pH.

- ^{59}Fe was not detected at low pH. It may indicate that the dissolution rate of iron from the fuel rod surface becomes high at low pH, so that iron cannot stay on the surface of fuel.

- At pH 9.3, the crud sample shows a much higher activity of ^{51}Cr than other samples. It suggests that chromium may deposit on the fuel rod selectively at a certain pH range.

- The increase of crud concentration in the coolant by reducing pH may be caused by the increase of dissolution rate from the fuel rod, because the crud activity shows the tendency to increase with lower pH. The chromium content in crud has been reported to be very sensitive to the hydrogen concentration in

the coolant, i.e., to the oxidizing or reducing nature of the coolant.

Table 5-1

Some Experimental Results
for Particulate Corrosion Products - Effect of pH[7)]

Chemistry	Crud Concentration (μg/kg H_2O)	Activity (GBq/kg crud)				
		^{60}Co	^{58}Co	^{51}Cr	^{59}Fe	^{95}Zr
Normal[a]	11[b] (5.4-19)	44 (15-70)	11 (3.0-22)	110 (18-230)	0.74 (0.37-1.1)	27 (2.2-96)
pH 7-8	60 (45-83)	410 (200-770)	63 (27-89)	920 (440-1400)	ND	350 (37-1100)
pH 9.3[c]	43	520	93	4400	ND	120
pH 11[c]	5.6	170	63	480	7.4	33
Low H_2, pH 10.5 (0 to 0.4 cm^3/kg)	48 (42-55)	230 (200-240)	27 (20-41)	740 (670-890)	4.4 (3.3-6.7)	100 (28-140)

a. Normal, pH 10 to 10.5 with LiOH; H_2 3 to 7 cm^3 (STP)/kg
b. Average and range of results
c. One sample only

Table 5-2 shows the effect of pH on specific activities. In fact, specific activities can provide information relating to the elemental deposition and release mechanism in the core. Judging from the table, it is evident that the increase of crud concentration in the coolant was caused by the increase of release rate from the fuel rod. The increase of specific activity also indicates that the apparent residence time in the core has considerably increased. It means that pH has a significant effect on the deposition rate from the coolant into the surface of fuel rod. The solubility of nickel ferrite may decrease quite abruptly by reducing the pH and increasing temperature, so it affects the incorporation rate of particles in the coolant onto the surface of fuel rod. It may be possible to explain the effect of pH on the crud transport with the change of solubility.

Table 5-2

The Effect of pH on the Specific Activities[7)]

Chemistry	Crud Concentration ($\mu g/H_2O$)	Specific Activity (GBq/kg)			
		^{60}Co	^{58}Co	^{51}Cr	^{59}Fe
Normal (pH 10~10.5)	11	11,000	46	2,037	3.0
pH 7~8	60	51,250	175	18,400	ND

Note) Specific activities were calculated from the weight percent of parent nuclide and activity in the crud.

As mentioned above, the effect of water chemistry on crud transport in the primary coolant system may be able to explain with the change of solubility due to the change of pH in the coolant. Table 5-3 shows the effect of pH and temperature on the solubility for nickel ferrite and magnetite.[11] The solubility and the temperature coefficient of solubility are affected by pH. The following are some important findings from the table.

- At pH higher than 7.5, it is evident that the temperature coefficient is positive. It means the solubility near the heated surface is higher than that in the bulk solution, which will cause the particle concentration near the heated surface to drop rapidly depending on the heat flux. For this reason, a thinner layer of deposits is thought to form on the fuel rod due to the decrease in deposition rate from the coolant onto the fuel rod. This can be also deduced from some test results which shows the possibility of deposit thinning on the surfaces of fuel rod by high pH operation in PWRs.

- On the contrary, the particle concentration can increase to some extent on cooler surfaces due to the decrease of solubility at lower temperatures. However, the deposition rate from the coolant onto the surfaces of out-core components appears to be governed by the crystallization of dissolved species present in the coolant incorporated into the outer oxide layer formed on the surface. Therefore, the deposition rate onto the cooler surfaces will decrease, and the release rate from the oxide film formed on the surfaces of out-core components into the coolant will increase at higher pH .

- By increasing pH from 7.5 to 8.4, the solubility of iron increases 3 to 5 times. It means the pH can also affect the release rate and deposition rate between the oxide film formed on the surface of metal and the dissolved species in the coolant. As mentioned in Chapter 2, the deposition rate from the coolant into the oxide film is thought to be proportional to the concentration of dissolved species in the coolant, and the concentration of dissolved species can be considered to be the same as the solubility of nickel ferrite in the steady state.

Table 5-3

Solubility of Nickel Ferrite and Magnetite[11)]

pH at 300℃	$Ni_{0.6}Fe_{2.4}O_4$ in $LiOH/B(OH)_3$ Solutions		Fe_3O_4 in Pure KOH Solutions (Calculated)	
	Solubility of Iron (μmole/kg)	Temperature Coefficient	Solubility of Iron (μmole/kg)	Temperature Coefficient
6.55	0.085	Negative	0.11	Zero
7.5	0.080	Positive	0.23	Positive
8.4	0.28	Positive	~1.2	Positive

Note) Solubility $\propto [H_2]^{1/3}$

However, the chemistry condition of the coolant is not uniform through the entire operating cyle. It means the temperature coefficient may change from negative to positive during the operation depending on the chemistry condition at BOL.

Table 5-4 shows the relationship between solubility and dissolution rate constant of magnetite into the high temperature water.[14)] At 10.2 of pH, the increase of temperature from 150 ℃ to 250 ℃ results in the increase of solubility from 0.39 to 1.26 μg Fe/kg solution. It causes only a four times increase in the solubility. However, the increase by more than 10 times in the dissolution rate constant is shown from the temperature change. It is not clear whether this big increase of the dissolution rate constant results from the temperature change or the solubility change.

The data measured at 250 ℃ may provide a clue to answer this question. The solubility increases more than seven times on changing the pH from 10.2 to 11.0, however, the dissolution rate constant shows a slight decrease. From this result, it can be said that the solubility does not affect the dissolution rate constant from the oxide film into the coolant. The change in temperature rather than solubility play the important role in the dissolution rate constant.

There is no data available to discuss the effect of pH on the deposition rate constant from the coolant onto the fuel rod. However, it may be assumed that the solubility change caused by the pH change does not have any influence upon the deposition rate constant. If there is change in the constant, it may be caused by the change in the solubility due to the change of temperature.

Table 5-4

Solubility and Dissolution Rate Constant of Magnetite in Water[14)]

pH	Temperature (℃)	Solubility (μg Fe/kg solution)	Dissolution Rate Constant (g Fe/cm^2 · s)
10.2	150	0.39	7.1×10^{-14}
10.2	200	0.65	2.3×10^{-13}
10.2	250	1.26	7.3×10^{-13}
11.0	250	9.14	6.26×10^{-13}

From the data discussed above, it is clear that pH must affect the incorporation rate of crud as particulates from the coolant into the surface of fuel rod. However, the deposition rate constant may not be affected by the change of solubility caused by the change of pH. Rather than pH, temperature seems to have a certain relationship with the deposition rate constant. In this report, the change of solubility due to the difference of temperature between bulk solution (coolant) and fuel cladding will be assumed to cause the change in the deposition rate constant from the coolant into the fuel rod.

It is possible to conclude that pH can also affect the release rate constant from the fuel rod into the coolant. However, some experimental data show a little effect of pH on the dissolution rate constant of magnetite. Moreover, the release mechanism from the fuel rod to the coolant is thought to be governed by erosion. Therefore, it is assumed that the release mechanism from the fuel rod into the coolant won't be affected by the change of pH in the coolant.

The deposition rate constant from the coolant into the surface of fuel rod, k_f will be modified by the following way in order to explain the different thickness of deposits for the different water chemistry conditions based on the above discussion. This approach is based on the simple assumption that the ratio of the solubilities between the bulk solution and the solution in contact with the fuel cladding gives the relative magnitude of the deposition rate constant. There is no theoretical background for this assumption, and there is no data available for this kind of discussion. However, the difference in the thickness of deposits formed on the surface of fuel rod caused by the different water chemistry environment can be partially explained by the following equation.

$$k_f^* = \frac{S^*(T_1)}{S^*(T_2)} \cdot \frac{S(T_2)}{S(T_1)} \; k_f \qquad \text{---------- (29)}$$

where T_1 : temperature of the bulk solution which is entering the core

T_2 : temperature at the cladding of fuel rod

$S(T_1)$, $S(T_2)$: solubility at T_1 and T_2 for the reference water chemistry

$S^*(T_1)$, $S^*(T_2)$: solubility at T_1 and T_2 for the modified water chemistry

The deposition rate from the coolant into the surfaces of out-core components appears to be governed by the crystallization rate. It means that the higher concentration of dissolved species due to the higher solubility may cause the higher deposition rate. Therefore, the effect of pH on the deposition rate can be explained by the same way as the deposition rate onto fuel rod. However, the release rate from oxide films into the coolant will decrease because of the increased concentration of dissolved species at the surfaces of oxide films.

In a similar way used to evaluate the deposition rate constant from the coolant onto the fuel rod, the release rate constant from oxide film formed on the steam generator tubes into the coolant, r_o, will be modified for different water chemistry conditions as follows,

$$r_o^* = \frac{S^*(T_2)}{S^*(T_1)} \cdot \frac{S(T_1)}{S(T_2)} \; r_o \qquad \text{---------- (30)}$$

where T_1, T_2 : temperature of the bulk solution and the surface of S/G tubing

$S(T_1)$, $S(T_2)$: solubility at T_1 and T_2 for the reference water chemistry

$S^*(T_1)$, $S^*(T_2)$: solubility at T_1 and T_2 for the modified water chemistry

Judging from the data given in Table 5-4, the release rate constant may be increased by more than the ratio of solubilities between in the bulk solution and in the solution contacted with the tube surface. However, the release rate constant will be modified under the same assumption as the case of deposition onto the fuel rod, because the data available at this moment are not enough to confirm the relationship between the solubility and the release rate constant.

For isothermal surfaces, no change in the release rate constant will be assumed. However, the concentration of dissolved species in the coolant will be affected by the change of pH. Therefore, the release rate from the oxide film into the coolant, which is proportional to the concentration of dissolved species in the coolant, will be directly affected by the change of pH.

The suitability of the method suggested here can be verified later by comparing the results calculated from the analytical model with the data found in nuclear power plants, if it is possible to acquire enough data on the solubility. A detailed comparison between the suggested method and the field data will remain for future study.

5-3 Hydrodynamic Effect

It is well-known that hydrodynamic characteristics affect greatly erosion corrosion behavior. There have been many efforts to describe the effect in terms of several hydrodynamic parameters. Hydrodynamic parameters can also affect the deposition mechanism from the coolant into the surfaces. In particular, the deposition mechanism of particulates surely be governed by the hydrodynamic parameters.

B. E. Brown et. al. measured the effect of flow rates on corrosion behavior of 304 stainless steel, and drew the following conclusions.[24)]

- In the case of laminar flow, increasing flow rates shift the breakdown potential in the noble direction, indicating increased stability of the passive film against pit initiation. However, this increase in stability of the passive film also causes the repassivation potential to become more active due to the increased potential difference between the more stable, passive surface and active pits.

- In the case of turbulent flow conditions, increasing the flow rate causes the breakdown and repassivation potentials to revert to values observed in stagnant solutions, suggesting that concentration gradients, which assist in the transport of reducing species to the surface, are reduced or eliminated.

- At the apparent transition between laminar and turbulent flow, the hysteresis between the breakdown potential and the repassivation potential is maximized. This suggests a maximum in the susceptibility to crevice corrosion.

- Increasing the flow rates in the laminar regime causes the net current density to decrease due to an increase in the limiting current density caused by shrinkage of the diffusiion boundary layer.

Bryan Poulson examined four parameters, including velocity, surface shear stress, intensity of turbulence, and mass transfer coefficient, to define the most important and useful hydrodynamic parameter which controls the occurrence and the rate of

erosion corrosion. He suggested the mass transfer coefficient is the most useful one for predicting the rate of erosion corrosion.[25]

It seems clear that increasing the flow rate will cause an increase in the rate of erosion corrosion. In fact, it is possible to imagine that the increased erosion rate in the high flow rate region will suppress activity accumulation. Contrary to this situation, the rate of activity accumulation might be dramatically increased in certain stagnant areas where particulates can be trapped. However, there is no adequate quantitative relationship which can cover the various situations found in nuclear power plants. Also, some loop test results show that there is a little evidence of erosion from the surface of out-core components. Therefore, the hydrodynamic effect will be excluded when evaluating corrosion rates from nuclear power plant components.

S. K. Beal presented a method for predicting the deposition of particles entrained in turbulent flow by considering Brownian diffusion, turbulent diffusion, and inertial effects under the assumption of the existnce of an equilibrium concentration of particles close to the wall.[26] He obtained a deposition coefficient in turbulent flow as follows,

$$\frac{1}{K_d} = \frac{1}{p\,v} + \frac{1}{K} \qquad \text{(31)}$$

where K_D : deposition coefficient

p : sticking probability

v : radial velocity of particle

K : transport coefficient

and

$$K = \frac{U\,f/2}{(1 - 13.73\sqrt{f/2})} \qquad \text{(32)}$$

where U : average fluid velocity

f : Fanning friction factor (= 1/4 Moody friction factor)

From the above equations, it is clear that the deposition coefficient becomes proportional to the average fluid velocity as pv becomes very large with respect to K. Therefore, the deposition rate of particulates in the turbulent flow increases with the flow rate.

Lister's result also shows a relationship for the deposition of dissolved species by crystallization in the nuclear steam generator tubes. From Eq. (22) and Eq. (28), it can be easily shown that the deposition rate from the coolant into the oxide film formed on the surface of Inconel tubes can be expressed as a function which is proportional to the flow rate inside the tubes, if the incorporation rate by crystallization mechanism into the outer oxide film is dominant compared to the deposition rate into the inner layer.

From the point of view of transport across the fluid film, the transport rate of dissolved species is expressed as a mass transfer coefficient multiplied by a concentration difference between the bulk fluid and the fluid in contact with the wall. If the concentration next to the wall is zero, the deposition coefficient will be equal to the mass transfer coefficient, and will follow a standard correlation with Reynolds number. In any case, the theoretical mass transfer coefficient should set an upper limit to the deposition coefficient, for material cannot be deposited more quickly than it can be transported across the fluid boundary layer.[27]

The erosion corrosion mechanism must be affected by the hydrodynamic characteristics, and the hydrodynamic effect can be expressed in terms of the mass transfer coefficient. Therefore, it may be reasonable to modify the input term of cobalt sources in order to include hydrodynamic characteristics. However, the experimental results show that the mass transfer coefficient varies with the flow conditions, the shapes of pipes, roughness of surface, etc. For example, the mass traansfer coefficient can be expressed for straight smooth pipes as follows,[25]

$$K = 0.014 \frac{D}{d} Re^{0.86} Sc^{0.37} \qquad \text{----------} \quad (33)$$

where D : diffusion coefficient

d : pipe diameter

The results obtained from bends show that smooth bends enhance mass transfer over the straight tube. As roughness develops, the enhancement increases to a factor of $0.71\ Re^{0.12}$ for a 180° bend in single phase flow. Therefore, the equation for the mass transfer coefficient should be modified for a 180° bend as follows,

$$K = 0.01 \frac{D}{d} Re^{0.98} Sc^{0.37} \quad \text{---------- (34)}$$

Moreover, the flow condition in the pipe can also affect the mass transfer process. At higher Reynolds numbers, when the tube also roughens, the enhancement will be expected to decrease compared to that at lower Reynolds numbers. Also, there are insufficient erosion corrosion data for the establishment of a relationship between the mass transfer coefficient and erosion corrosion rate in the high temperature flow conditions expected in the nuclear primary system. For these reasons, it is not easy to reflect the hydrodynamic effect into complicated system such as nuclear primary coolant system, even though it is possible to infer some relationships for the mass transfer coefficient for the system.

It is clear that hydrodynamic characteristics also have a great effect on the deposition process of particles into the surface of out-core components. In this case, the deposition process may be expressed by the mass transfer coefficient. Some experimental result shows that the mass transfer coefficient can be used to express the deposition mechanism of particles in the same way used in the erosion corrosion mechanism.

However, some evidence obtained from the radiochemical analysis strongly suggests that the deposition process of radioactive materials from the coolant into the oxide film formed on the surface of out-core components may be governed by the crystallization process of dissolved species in the coolant into the outer oxide film. If this is true, it is not appropriate to express the deposition mechanism in terms of the mass transfer coefficient, even though Lister shows that the crystallization process in the steam generator tubes is enhanced by the flow rate.

As mentioned above, it is not easy to derive a quantitative relationship which describes the hydrodynamic effect on the erosion corrosion mechanism of the out-core materials, and the deposition mechanism of radioactive material from the coolant into the oxide film formed on the out-core surfaces. Therefore, the hydrodynamic effect will be not considered for the analysis of deposition mechanism of cobalt in PWR primary coolant systems.

5-4 Heat Flux

Heat flux may be considered a parameter that affects ^{60}Co deposition in the primary coolant system. It is possible to imagine that local boiling near the surface of a fuel rod enhances the deposition rate of particles by concentrating them near the surface. It is also possible to imagine that a change of solubility in the coolant contacting with the fuel rod may cause the change in the concentration of particles, and thereby the change of deposition rate. If the former process is dominant, the deposition rate from the coolant onto the fuel rod will always increase. However, in case the latter process is dominant, the deposition rate will change depending on the solubility at the temperature of fuel cladding. If the temperature coefficient of solubility is positive, then the increased solubility at the fuel cladding will decrease the concentration of particles, and lead to the decrease of deposition rate onto the fuel rod.

Table 5-5 shows the deposition data onto the fuel rod found from Beznau unit 1 cycle 3 core, which demonstrates the effect of heat flux.[10] In this table, the following conclusions regarding the deposition mechanism onto the fuel rod can be made :

- The deposit thickness formed on the surface of fuel rod shows the dependency of heat flux across the fuel rod surface. Even though a large variation in the data was found, it looks possible to conclude that the heat flux enhances the deposition rate of crud from the coolant into the surface of fuel rod under the chemistry condition of the Beznau unit 1 cycle 3 core.

- The compositions of chromium and cobalt are much higher at high power than at low power. It may suggest the possibility of a selective deposition process depending on the heat flux. Maybe, these observed results can be explained by the concentrating effect of ions at the heated surface.

- The chemistry condition in the coolant is not given. Therefore, it is impossible to conclude that the weight of deposit will increase under any chemistry

Table 5-5

Average Crud Compositions from Beznau Unit 1 Cycle 3 Core (NOK)[10)]

	Low Power (3~4 kW/ft)	High Power (6~7 kW/ft)
Deposit Thickness, mg/dm^2 Average (Range)	2.1 (0.6~7.5)	10.8 (0.6~48)
Iron (wt% ± σ)	45.1 ± 19.6	32.3 ± 8.4
Nickel (wt% ± σ)	21.4 ± 9.6	24.1 ± 8.2
Chromium (wt% ± σ)	0.78 ± 0.23	2.46 ± 1.09
Manganese (wt% ± σ)	0.13 ± 0.01	0.19 ± 0.06
Cobalt (wt% ± σ)	< 0.03	0.06 ± 0.02
Nickel/Iron	0.47	0.75

conditions with the increase of heat flux.

The deposition process on cool surfaces such as steam generator tubes may be different from that on heated core surfaces. There is no boiling on cool surfaces. Unlike the deposition process on heated surfaces, deposition on the cool surfaces is controlled by the crystallization process of dissolved species. Therefore, the deposition rate onto the cool surfaces surely depends on the concentration of dissolved species at the cool surfaces.

Some deposition data on cool surfaces obtained from in-reactor loop experiments are shown in Table 5-6. It is not clear if the coolant condition was the same for the three separate runs or whether the decay rate was corrected for the comparison. However, it is possible to infer some characteristics of the deposition process onto the cool surfaces from the relative activity of ^{60}Co and ^{58}Co in the coolant and the trapped activities in the cooler and the ion exchange column.

- First of all, the activity trapped on the cool surfaces shows the high deposition rate of ^{60}Co compared to that of ^{58}Co judging by the activity of those isotopes found in the coolant or ion exchange column. In fact, the ratio of two isotopes may have the value between the ratios found on the ion exchange column and that found in the insolubles in the coolant if we assume the contribution of particle deposition.

- From the experimental condition (pH 10 to 10.5 with LiOH), the temperature coefficient of solubility is believed to be positive. If that is true, the particle concentration on the cooled surface presumably increases to some extent. The increased concentration of particles enhances the possibility of agglomeration. Thus, the contribution of particle deposition to the deposition process may be increased. However, the experimental result shows the opposite tendency. It may support that deposition onto cool surfaces is governed by crystallization of dissolved species in the coolant.

- This might be also explained by the deposition and release processes. The activity trapped on the ion exchanger is thought to represent the accumulated activity of dissolved species. If there were no release mechanism from the cool surfaces, then the ratio between ^{60}Co and ^{58}Co found on cool surfaces must be smaller than that found on the ion exchange column. Therefore, the release of ^{60}Co from oxide films deposited on cool surfaces into the coolant must affect the relative activity deposited on the surfaces of cooler. And this situation may be only possible when the radioactive isotopes recently trapped are preferentially released by dissolution from the cool surfaces into the coolant.

Table 5-6

Some Deposition Data of Radioactivity on Cool Surfaces[7)]

Cooler Material	Activity on Surfaces of Cooler (kBq)			Activity on Ion Exchange Column (kBq)			Activity in the Coolant	
							Soluble	Insoluble
	^{60}Co	^{58}Co	$^{60}Co/^{58}Co$	^{60}Co	^{58}Co	$^{60}Co/^{58}Co$	$^{60}Co/^{58}Co$	$^{60}Co/^{58}Co$
Stainless Steel	1,330	107	12.4	3,700	590	6.3	5.5	3.1
Stainless Steel	155	13.3	11.7	407	66.6	6.1		
Zircaloy	192	32.6	5.9	814	185	4.4		

In-pile loop studies of the effect of PWR coolant pH show that S/G tubing deposition at low pH is increased, while at high pH it is decreased relative to contiguous adiabatic sections of the same tubing.[28)] These authors also suggest that the change of solubility due to the temperature change can affect the deposition and release process of radioactive material on the cooled surfaces.

The effect of heat flux on the deposition rate onto the heated surfaces is quite apparent, and it might be possible to explain the effect in terms of the difference of solubility on the heated surfaces to some extent by using Eq. (29). The release mechanism from the fuel rod is believed to be controlled by erosion corrosion, therefore, no effect of heat flux on the release rate will be assumed.

Even though it will be assumed a constant heat flux in the core region in this report for the convenience of analysis, it is possible to analyze the crud concentration for each fuel assembly, or for each position on the fuel rod by considering the change of solubility due to the change of cladding temperature. This effect can be explained by the solubility change. There must be a concentration effect of particles near the fuel cladding induced by the local boiling, however, the effect from the local boiling will not be considered in this report.

It is impossible to imagine any special mechanism which can promote or suppress the deposition rate or release rate in the steam generator tubing except the change of solubility. No effect on the deposition rate constant onto cool surfaces is assumed in this report, because there is no definitive evidence which shows the change in the deposition rate constant. However, the release rate constant will be adjusted by using Eq. (30).

The difference between the measured data and the evaluated data by modifying the chemistry condition may be explained in the terms of local boiling effect. However, it is impossible to find enough data for the evaluation of local boiling effect on deposition at this time. Therefore, it will be reserved for a future work.

5-5 Surface Treatment

In order to reduce the accumulation of ^{60}Co radioactivity in the primary coolant system, surface treatment methods can be very effective. Surface treatment methods have recently been studied, and most of data have been published by EPRI.

Surface treatment methods may be classified into three categories as follows:

- surface smoothing
- passivation
- coating

5-5-1 The Effect of Surface Smoothing

Surface roughness plays an important role in the process of deposition by enhancing the mass transfer coefficient in the flow. Therefore, a key step for the surface treatment is to smooth the surface of component to be exposed to primary coolant containing ^{60}Co. Electropolishing and mechanical polishing are widely being utilized to reduce the roughness of structural materials used in the nuclear power plant.

Electropolishing has proven to be a cost-effective method for smoothing large runs of BWR circulating piping. ^{60}Co pickup measurements on BWR recirculation piping show that electropolishing can reduce radiation fields by about a factor of two. Further reductions in field buildup may be achieved if piping is first mechanically smoothed.[28)]

Electropolishing can also be used to reduce radiation fields in PWRs. With or without prior mechanical polishing and with or without passivation, electropolishing was shown to have a dramatic effect on lowering the rate of activity buildup on

the manway seal plates exposed to reactor coolant at the Chinon B1 pressurized water reactor. A factor of four to five improvement for ^{60}Co was noted compared to the buildup rate on as-received surfaces.[31]

Mechanical polishing by itself lowers the radiation buildup rate somewhat (about 35% for ^{60}Co). However, it does not produce the level of improvement achieved with electropolishing, even though the surface roughness of mechanically polished surfaces can be as smooth as that of electropolished ones (as measured by profilometry).[31]

5-5-2 The Effect of Passivation

Plant data suggest that electropolishing followed by preoxidation in high-oxygen water reduces surface activity by some 30% over that achieved by electropolishing only. Pretreatment with EDTA was found to be effective in laboratory loop experiments in BWR water. Zinc injection passivation has been implemented at a few BWRs. Zn atoms appear to occupy the same cation sites as Co atoms in the growing oxide films. The continuous injection of low levels of zinc acts as an effective barrier against ^{60}Co.[28]

Passivation of as-received surfaces does not seem to result in any discernible improvement in the radiation buildup rate.[31] However, a further reduction in buildup rate was achieved by passivation following electropolishing. The improvement achieved with the Centec preoxidation passivation method provides an additional 8 to 50% improvement for the principal radioisototes constituting the radiation dose, while the Framatome passivation yielded an additional improvement of 12 to 20%.[31]

5-5-3 Coating Effect

Laboratory loop experiments show that metallic films offer the potential for achieving subsantial improvements over currently available technology. Palladium, nickel, and chromium films have performed best in both simulated PWR and BWR coolant chemistry.

EPRI has evaluated various pretreatment methods. Of the forty samples of type 304 stainless steel tubing exposed to simulated PWR coolant containing ^{60}Co, the two treated with "SRI-Pd deposition" showed the least deposition. Coefficents of parabolic kinetics used to fit the data showed that these samples activated to only 3.8% of the untreated controls. The next lowest were "Dayton-Tinker Ni-P" at 11% of the controls. Samples treated with "University of Pitsburgh chromate" and "Foster-Wheeler chromate/dichromate" showed no improvement.[30)]

After installation of the replacement RHR system piping at Diablo Canyon Unit 2, EPRI examined the effect of chromium coating on recontamination. The results are presented in Table 5-7.[32)]

However, the recent study on chromium coating of S/G manway seal plates showed reduction factors of ~10 at Millstone 2. Significant numbers of chromium-coated manway seal plates will be installed in SG at Duke Power and Pacific Gas & Electric PWRs.

5-5-4 Surface Treatment Effects on ^{60}Co Deposition

Judging from the above results, surface smoothing may affect the deposition process. Even though it may be possible to reduce the corrosion rate of base metal, it is more likely to reduce the deposition rate of corrosion products onto the smoothed surface. Because surface smoothing doesn't provide any protective layer for preventing corrosion, it will be modelled by adjusting the deposition rate constant from the coolant into the surfaces of treated components in this report.

Table 5-7

Recontamination Results of RHR System Piping
After Replacment at Diablo Canyon Unit 2

Spool ID	Surface Treatment	Specific Activity of ^{60}Co, $\mu Ci/cm^2$	^{60}Co Reduction Factor
RHR-8	EP + CR + PV	1.6E-02	3.50
RHR-7	EP + CR	2.3E-02	2.43
RHR-10	EP + PV	2.4E-02	2.33
RHR-9	EP Only	2.9E-02	1.93
RHR-AR	As Received	5.6E-02	1.00

However, passivation is supposed to produce the protective film on the surfaces of treated components. It is not clear if this film plays a role in the retardation of deposition and release process across the film or if it prevents corrosion of the base metal. In this report, the corrosion rate will be assumed to be reduced by the protective film which is formed on the electropolished surfaces by passivation. Without electropolishing, it appears that passivation doesn't have any positive effect on the buildup of radioactivity. Therefore, no effect of passivation will be assumed when it doesn't follow electropolishing.

The protective coating formed on the electropolished surfaces of components will be assumed to suppress the corrosion rate just like the protective film formed by passivation. Considering the experimental condition for the preparation of samples presented in the reference 30, it seems that electropolishing was not performed prior to coating palladium onto samples, or electroplating Ni-P onto a sample. Therefore, the protective coating will be assumed to have a reduction effect on the buildup of radioactivity irrespective of the pre-treatment by electropolishing.
The Diablo Canyon Unit 2 test result shows that chromium coating itself has the

similar effect to that of passivation. But it shows chromium treatment following by passivation provides an additional improvement factor of 1.44. Due to the lack of information, it looks too early to conclude that passivation will enhance the effect of chromium coatings. However, it may be possible to conclude that the film formed by passivation plays an independent role in reducing the buildup of radiation of the chromium coatings, or has a synergistic effect with them.

Based on the above discussion, surface treatment effects presented in Table 5-8 can be applied for the evaluation of ^{60}Co accumulation on the treated surfaces. In this table, the reduction factor of chromium coating may be re-evaluated in order to reflect the recent results of EPRI.

Table 5-8

Surface Treatment Effects on the Crud Transport
in the PWR Primary Coolant System

Surface Treatment	Reduction Factor	Crud Transport Process	Comments
Mechanical Polishing	1.5	Deposition Rate	Based on ^{60}Co[31]
Electropolishing	4.0	Deposition Rate	Based on ^{60}Co[31]
Preoxidation (With Electropolishing)	1.2	Corrosion Rate	Based on ^{60}Co[32]
Chromium Coating	1.3	Corrosion Rate	Based on ^{60}Co[32]
Palladium Coating	26.3	Corrosion Rate	Based on ^{60}Co[30]
Ni-P electroplating	9.1	Corrosion Rate	Based on ^{60}Co[30]

5-6 Out-Core Deposition Model

5-6-1 Thickness of Deposits Forming on Out-Core Components

As examined above, the deposition mechanism of crud from the coolant onto the out-core surfaces is controlled by the crystallization process of ions into the outer layer of oxides. Therefore, let's suppose the deposition rate from the coolant into the oxide layer formed on the surface of out-core component is proportional to the concentration of dissolved species present in the coolant. Then, the change in the weight of oxide film formed on the surface can be calculated as follows:

$$\frac{dW_o(t)}{dt} = k_c - r_o\, W_o(t) + k_d\, C_d \qquad \text{---------- (35)}$$

where $W_o(t)$: weight of metal components contained in the oxide film formed on the surface of out-core components at time t, g/m^2

k_c : corrosion rate constant, $g/m^2 \cdot s$

r_o : oxide film release rate constant, s^{-1}

k_d : deposition rate constant, m/s

C_d : concentration of dissolved metal ions in the coolant, g/m^3

In Eq. (35), the concentration of dissolved metal ions in the coolant can be assumed the same as the solubility of nickel ferrite. So, it is possible to treat C_d as constant unlike the concentration of particulates in the coolant. Then, the solution to Eq. (35) becomes

$$W_o(t) = e^{-r_o t}\, [\int e^{r_o t} \cdot (k_c\, t + k_d\, C_d)\, dt + C\,]$$

$$= \frac{k_c + k_d\, C_d}{r_o} + C\, e^{-r_o t} \qquad \text{---------- (36)}$$

where C is constant.

From the initial condition of the weight of oxide film, C can be shown as follows,

$$C = -\frac{k_c + k_d C_d}{r_o}$$

Therefore, $W_o(t)$ becomes

$$W_o(t) = \frac{k_c + k_d C_d}{r_o} (1 - e^{-r_o t}) \qquad \text{---------- (37)}$$

In the above equation, k_d is the only rate constant which has to be evaluated.

5-6-2 Evaluation of Deposition Rate Constant

In this model, the thickness of corrosion oxides formed on the surface of base metal has reached its equilibrium value. It may be not true in a closed system, because the higher concentration of particulates in the coolant due to the higher release rate will cause the deposition rate of particulates from the coolant onto the oxide layer to increase. However, some of corrosion products are constantly being removed from the nuclear primary coolant circuit by the purification system. This suggests the removal rate of corrosion products can be equal to the corrosion rate if the removal flow rate is high enough.

In order to evaluate the value of k_d, the measured equilibrium thickness must be known. A deposit of 7 mg · Fe/cm^2 was reported as the heaviest observed under any conditions tested in Ref. 3. However, this value is for the heat transfer surfaces. In fact, the equilibrium thickness is thought to be dependent on the type of base metals, heat flux, water chemistry, etc. There is no data available for the equilibrium thickness right now. Therefore, let's depend on the Lister's models to evaluate the equilibrium thickness.

The oxide film growth expression for stainless steel by Lister is given by the following equation as discussed in Chapter 2.

$$m(t) = \sqrt{1.73\times10^{-5}\, t} \quad g/m^2 \qquad \text{---------- (38)}$$

By assuming the same thickness of inner oxide layer as that of outer oxide layer, the oxide film growth equation on the non-isothermal surface of Inconel steam generator tubing can be modified as follows,

$$m(t) = \sqrt{3.31\times10^{-7}\, t} \quad g/m^2 \qquad \text{---------- (39)}$$

Eq. (38) and (39) for the thickness of oxides are surely a function of time, so they never reach the equilibrium values. Therefore, the time at which the quasi-equilibrium state is expected to be reached will be evaluated from the Eq. (37) by putting $e^{-r_o t}$ as 10^{-2}. The values of "t" for stainless steel and Inconel-600 are estimated as follows,

$t = 1.11\times10^7$ *sec* (128 *days*) for stainless steel

$t = 8.28\times10^7$ *sec* (959 *days*) for Inconel-600 S/G tubing

Even though the selection of the value for $e^{-r_o t}$ was arbitrary, the above results show quite good agreement with the some experimental results. The measurement results of alloy weight change for stainless steel 304L and Inconel-600 after exposing coupons to coolant up and down stream from the filter show a continual weight loss for Inconel-600, but no change for stainless steel during exposure, which suggests a longer time is required to reach the equilibrium state for Inconel-600 than stainless steel.[18] Equilibrium thicknesses, W_{eq}, calculated from Eq. (38) and (39) at the above-given time are

$W_{eq} = 13.86$ *g as metal oxides*$/m^2$

$= 9.70$ *g as metal components*$/m^2$ for stainless steel

$W_{eq} = 5.24$ *g as metal oxides*$/m^2$

$$= 3.66 \quad g \text{ as metal components}/m^2 \quad \text{for Inconel-600 S/G tubing}$$

The thicknesses of metal oxides obtained by Eq. (38) and (39) were converted to the thicknesses of metal components by considering the weight ratio of metal components contained in the metal oxides formed on the surface of base metals.

By assuming that the concentration of dissolved metal ions in the coolant is the same as the solubility of nickel ferrite in the coolant, it is possible to estimate the deposition rate constant from Eq. (37). The solubility of nickel ferrite obtained by Y. L. Sandler and R. H. Kunig at 7.4 of pH, 300 ℃, and 0.75 cm^3/min of flow rate will be adopted as the ionic concentration in the coolant. Then, C_d becomes

$$C_d = 0.08 \quad \mu mol \text{ of } Fe/kg + 0.003 \quad \mu mol \text{ of } Ni/kg$$

$$= 4.64\times10^{-6} \quad g/kg \quad = 4.64\times10^{-3} \quad g/m^3$$

The values of k_d for stainless steel and for Inconel steam generator tubing estimated from Eq. (37) are as follows,

$$k_d = 8.53\times10^{-4} \quad m/s \quad \text{for stainless steel}$$

$$k_d = 2.28\times10^{-6} \quad m/s \quad \text{for Inconel steam generator tubing}$$

As expected from Eq. (37), the values of k_d are strongly dependent on the thicknesses of the steady state oxides. Moreover, the corrosion rate constants and release rate constants can be a limiting factor for the minimum thicknesses of oxides. For example, W_{eq} must be larger than k_c/r_o. If it were possible to find the measured data for W_{eq}, it would be much easier to decide reasonable values of k_d by re-evaluating corrosion and release rate constants. Even though the above values are estimated arbitrarily by selecting the Lister's model to calculate the vales of W_{eq}, they look quite reasonable based on findings from several experiments. As discussed in Chapter 2, the deposition rate on stainless steel is surely much higher than that on the Inconel-600. Also, the continual loss of

weight found in the coupon of Inconel-600 exposed into the PWR environment can be explained by these values. Therefore, the above values of k_d will be used for the analysis of ^{60}Co deposition in the primary coolant system of PWRs in this report.

5-6-3 Evaluation of ^{60}Co Concentration in the Primary Coolant System

In order to evaluate the concentration of ^{60}Co atoms in the oxide layer, let's obtain an equation for the accumulation rate of ^{60}Co atoms in the oxide film. In the previous section, it focused on the evaluation of rate constants based on the ionic deposition into oxide layer formed on structural materials by cryatallization. However, this assumption may cause excessive accumulation of particulates in the coolant. Therefore, particulate deposition into the oxide layer should be also considered in order to simulate the transport of crud in the primary coolant system. In this report, the particulate deposition rate constant will be assumed to be proportional to the ionic deposition rate constant. Assuming particulate deposition from the coolant into the oxide layer, Eq. (37) should be modified as follows,

$$W_o(t) = \frac{k_c + k_d C_d + f k_d C_p}{r_o} (1 - e^{-r_o t}) \qquad \text{-------- (37-1)}$$

where f means the rate constant ratio between particulate deposition and ionic deposition. If f approaches to zero, then it means no particulate deposition occurs in the primary coolant system. The value of f will be evaluated from the concentration of particulates found in the primary coolant system.

Since ^{60}Co atoms are not released from the base metal to the oxide layer, the change in the number of ^{60}Co atoms present in the deposit can be expressed as a following equation.

$$\frac{d\{n_o(t)\ W_o(t)\}}{dt} = k_d C_d n_d(t) - r_o (1+e) n_o(t) W_o(t)$$

$$- \lambda \; n_o(t) \; W_o(t) \; + f \, k_d \; C_p \; n_p(t) \qquad \text{---- (40)}$$

where $n_o(t)$: number of ^{60}Co atoms contained in a gram of metal components in the oxide film at time t

$n_d(t)$: number of ^{60}Co atoms contained in a gram of dissolved metal ions in the coolant at time t

$n_p(t)$: number of ^{60}Co atoms contained in a gram of particulates in the coolant at time t ($n_p = n_{po}$ in the hot leg side, and $n_p = n_{pi}$ in the cold leg side)

e : cobalt enrichment factor into the released ions

The solution to Eq. (40) is

$$n_o(t) \; W_o(t) = e^{-\{r_o (1+e) + \lambda\} t} \times \left[\int k_d \; C_d \; n_d(t) \; e^{\{r_o (1+e) + \lambda\} t} \, dt + C \right] \qquad \text{-- (41)}$$

Since $n_d(t)$ is an unknown function of time t, it is impossible to get an analytical solution to Eq. (41). However, it may be possible to assume $n_d(t)$ as constant from the fact that the activity deposited on the oxide film has been reached at a nearly constant value when some time elapsed after start-up of the plant. For example, the accumulated activity of ^{60}Co in the steam genertor tubing is expected to increase to 5.68 mCi/m^2 in the first year, however, no more than 10% increase is expected in the following year from the Lister's model. Therefore, let's assume that $n_d(t)$ is constant in order to evaluate the value of k_d from the measured activity at steady state. Then, Eq. (41) can be expressed as follows,

$$n_o(t) \; W_o(t) = \frac{k_d \; C_d \; n_d(t) + f \; k_d \; C_p \; n_p(t)}{r_o \; (1+e) \; + \; \lambda} \times \{1 - e^{-\{r_o (1+e) + \lambda\} t}\} \qquad \text{---------- (42)}$$

Now, it is possible to calculate the concentration of ^{60}Co atoms present in the

primary coolant circuit. From Eq. (42), the number of ^{60}Co atoms per gram oxide layer (as metal components) formed on the surface of out-core components can be obtained from the following equation if it is possible to find $n_d(t)$ and $n_p(t)$.

$$n_o(t) = \frac{k_d\, C_d\, n_d(t) + f\, k_d\, C_p(t)}{\{r_o\,(1+e)+\lambda\}\, W_o(t)} \times \left[\, 1 - e^{-\{r_o\,(1+e)+\lambda\}\, t} \,\right] \qquad \text{---------- (43)}$$

In order to evaluate $n_d(t)$ and $n_p(t)$ in the above equation as a function of t, it is necessary to look at the whole primary coolant system. If we assume the concentration of particulates in the coolant entering the core is C_{pi}, and that in the coolant leaving the core is C_{po}, then C_{po} can be expressed as follows from the material balance of particulates in the coolant,

$$C_{po} = C_{pi} - \frac{A}{F}\, k_f\, C_{pi} + \frac{A}{F}\, r_f\, W_F - \Delta C_d \qquad \text{---------- (44)}$$

where C_{pi} : concentration of particulates in the coolant entering the core, g/m^3

C_{po} : concentration of particulates in the coolant leaving the core, g/m^3

ΔC_d : difference in the ionic concentration in the coolant between entering the core and leaving the core, g/m^3

A : total area of fuel rod surface, m^2

F : flow rate of coolant, m^3/s

Substituting Eq. (18) with W_F in Eq. (44), then gives

$$C_{po} = C_{pi}\,(1 - \frac{A}{F}\, k_f\, e^{-r_f\, t}) - \Delta C_d \qquad \text{---------- (45)}$$

In the same way, it is possible to derive the equation for ^{60}Co atoms present in the coolant particulates entering and leaving the core from the material mass balance. However, the temperature coefficient of solubility should be considered to set up a equation for the mass balance of ^{60}Co atoms. If it is positive, for example,

particulates will be dissolved into metal ions in order to compensate for the increased solubility in the core. However, if it is negative, metal ions will crystallize to form particulates. For the positive temperature coefficient of solubility, therefore, the equation can be expressed as follows,

$$n_{po}\, C_{po} = n_{pi}\, C_{pi} - \frac{A}{F} k_f\, n_{pi}\, C_{pi} + \frac{A}{F} r_f\, n_f\, W_F - \Delta C_d\, n_{pi}$$

$$= n_{pi}\, C_{pi} - (\frac{A}{F} k_f\, C_{pi} - \Delta C_d)\, n_{pi}$$

$$+ \frac{A}{F} k_f\, n_f\, C_{pi}\, (1 - e^{-r_f t}) \qquad \text{---------- (46)}$$

where n_{pi} : number of ^{60}Co atoms per gram particulates as metal components in the coolant entering the core, *#/g*

n_{po} : number of ^{60}Co atoms per gram particulates as metal components in the coolant leaving the core, *#/g*

n_f : number of ^{60}Co atoms per gram deposits as metal components formed on the surface of fuel rod, *#/g*

In equation (46), it is manifest that the number of ^{60}Co atoms per gram particulates in the coolant will change while going through the core. In order to solve this equation, let's define two variables as follows,

$$g_1 = \frac{C_{pi}}{C_{po}} (1 - \frac{A}{F}\, k_f) - \frac{\Delta C_d}{C_{po}} \qquad \text{---------- (47)}$$

$$g_2 = \frac{A}{F}\, k_f\, n_f \frac{C_{pi}}{C_{po}} (1 - e^{-r_f t}) \qquad \text{---------- (48)}$$

then, Eq. (46) can be simplified as follows

$$n_{po}(t) = g_1\, n_{pi}(t) + g_2 \qquad \text{---------- (49)}$$

In Eq. (48), n_f can be expressed from Eq. (18) and Eq. (20) as follows,

$$n_f = \frac{n_a}{W_F} = \frac{n}{(1 - e^{-r_f t})} \times \left[\frac{\sigma_{th}\,\psi_{th} + \sigma_{ep}\,\psi_{ep}}{\lambda + r_f} - \frac{\sigma_{th}\,\psi_{th} + \sigma_{ep}\,\psi_{ep}}{\lambda} e^{-r_f t} + \frac{r_f\,(\sigma_{th}\,\psi_{th} + \sigma_{ep}\,\psi_{ep})}{\lambda\,(\lambda + r_f)} e^{-(\lambda + r_f)\,t} \right] \quad \text{--- (50)}$$

In order to obtain the value of n_f, the number of parent target nuclei per gram deposit, n, should be obtained. In this report the uniform distribution of the released metal components is assumed. Actually, it is not true judging from the measured data for the compositions of fuel deposit, particulates in the coolant, and dissolved species in the coolant. However, the assumption may result in a conservative evaluation of ^{60}Co activity, because the enrichment of cobalt elements in the released solution was modelled. Therefore, n can be evaluated from the following expression.

$$n = \frac{N_A}{M} \frac{\text{total weight of released cobalt}}{\text{total weight of released metals}} = \frac{N_A}{M} \frac{\Sigma\, R'_{Co}(t)}{\Sigma\, R'(t)} = \frac{N_A \{\Sigma_i\,(A_i\, f_{Co}\,(1 + e))_i\, R'_i(t)\}}{M \{\Sigma_i\,(A_i)\, R'_i(t)\}} \quad \text{---------- (51)}$$

where N_A : Avogadro's number (= 6.024×10^{23})

M : atomic mass number of ^{59}Co

f_{Co} : weight fraction of ^{59}Co in the base metal (0.0007 for stainless steel,

0.0004 for Inconel-600, and 0.60 for Stellite-6)

e : cobalt enrichment factor in the solution (0.67 for stainless steel, 1.37 for Inconel-600, and 0 for Stellite-6)

A_i : surface area of base metals contacted with the primary coolant

i : type of base metals

and $R'_i(t)$, which is the total weight of metal components released from the metal oxides formed on the base metal i, is given by

$$R'_i(t) = k_{c,i}\{t - \frac{1}{r_{o,i}}(1 - e^{-r_{o,i}t})\} \quad \text{---------- (52)}$$

In order to obtain the value of $n_{pi}(t)$ and $n_{po}(t)$, C_{pi} and C_{po} should be evaluated. Let's assume that particulates in the coolant entering the out-core system will be transformed into dissolved species in order to compensate for the removal of dissolved species by purification and deposition in the out-core components, and dissolved species in the coolant leaving the out-core system will be transformed into particulates in order to compensate for the added dissolved species by dissolution from the out-core components. Then, it is possible to get analytical solutions for C_{pi} and C_{po}. Under these assumptions, the concentration of particulates present in the coolant entering the core can be expressed as follows,

$$C_{pi} = C_{po} + \frac{R_t(t) - D_i(t) - D_p(t) - P_t(t)}{F} + \Delta C_d \quad \text{-- (53)}$$

where $R_t(t)$: total release rate of metal components from the out-core components into the coolant, g/s

$D_i(t)$: total deposition rate of metal ions from the coolant onto the out-core components, g/s

$D_p(t)$: total deposition rate of particulates from the coolant onto the out-core components, g/s

$P_t(t)$: total removal rate of metal components from the coolant by purification systems, g/s

In the above equation, $R_t(t)$, $D_t(t)$ and $P_t(t)$ can be shown as follows,

$$R_t(t) = \Sigma_i \{A_i R_i(t)\}$$

$$= \Sigma_i \{A_i (k_{c,i}+k_{d,i} C_d) (1 - e^{-r_{o,i} t})\} \quad \text{---------- (54)}$$

where A_i : surface area of base metal i which contacts with the coolant, m^2

$k_{c,i}$: corrosion rate constant of base metal i, $g/m^2 \cdot$ sec

$k_{d,i}$: deposition rate constant of metal ions onto base metal i, g/m

$r_{o,i}$: release rate constant from the oxide formed on the surface of base metal i into the coolant, s^{-1}

By assuming that there is no change in the deposition rate constant between the hot leg side and the cold leg side, $D_i(t)$ and $D_i(t)$ can be obtained as follows,

$$D_i(t) = \Sigma_i (A_i k_{d,i} C_d) \quad \text{---------- (55)}$$

$$D_p(t) = \Sigma_i (f k_{d,i} C_p)$$

$$= \Sigma_i \{f (A_i)_c k_{d,i} C_{pi}\} + \Sigma_i \{f (A_i)_h k_{d,i} C_{po}\}$$

$$= K_{pi} C_{pi} + K_{po} C_{po} \quad \text{---------- (56)}$$

where $k_{d,i}$: deposition rate constant from the coolant into the oxide film formed on the surface of base metal i, m/s

$(A_i)_c$: surface area of base metal i contacting the coolant in the cold leg side, m^2

$(A_i)_h$: surface area of base metal i contacting the coolant in the hot leg side, m^2

C_d : concentration of dissolved species as metal ions in the coolant, g/m^3

and K_{pi} and K_{po} are

$$K_{pi} = \Sigma_i \{f (A_i)_c \, k_{d,i}\}$$

$$K_{po} = \Sigma_i \{f (A_i)_h \, k_{d,i}\}$$

In Eq. (53), the total removal rate by the purification system should be divided into two components. One is for metal ions, and another is for particulates as follows,

$$P_t(t) = P_{p,t}(t) + P_{d,t}(t)$$

where $P_{p,t}(t)$: total removal rate of particulates present in the coolant by the purification systems, g/s

$P_{d,t}(t)$: total removal rate of dissolved metal ions present in the coolant by the purification system, g/s

In the above equation, $P_{p,t}(t)$ and $P_{d,t}(t)$ can be obtained from a decontamination factor of the purification system and a flow ratio going through the purification system as follows,

$$P_{p,t}(t) = \left(\frac{DF_p - 1}{DF_p}\right) C_{po} \cdot F \cdot r_p \qquad \text{---------- (57)}$$

$$P_{d,t}(t) = \left(\frac{DF_d - 1}{DF_d}\right) C_d \cdot F \cdot r_d \qquad \text{---------- (58)}$$

where DF_p, DF_d : decontamination factors of the purification system for particulates and metal ions

r_p, r_d : ratio of the purification flow to the coolant flow

F : flow rate of the coolant, m^3/s

Then, C_{pi} and C_{po} can be solved from Eq. (45) and Eq. (53) as follows,

$$C_{pi} = \frac{R_t(t) - D_i(t) - P_{d,t}(t) + \Delta C_d\ (K_{DF}+K_{po})}{F - f_1(t)\ (F-K_{DF}-K_{po}) + K_{pi}} \qquad \text{-------- (59)}$$

$$C_{po} = \frac{f_1(t)\{R_t(t)-D_i(t)-P_{d,t}(t)+\Delta C_d\ (K_{DF}+K_{po})\}}{F - f_1(t)\ (F-K_{DF}-K_{po}) + K_{pi}} + \Delta C_d \qquad (60)$$

where $f_1(t)$ and K_{DF} are defined as follows,

$$f_1(t) = 1 - \frac{A}{F}\ k_f\ e^{-r_f t} \qquad \text{---------- (61)}$$

$$K_{DF} = F\ r_p\ (\frac{DF_p - 1}{DF_p}) \qquad \text{---------- (62)}$$

In order to obtain the relationship among n_{pi}, n_{po}, n_d and n_o, Eq. (43) and (49) are not enough. Therefore, some relationships are derived from the assumed exchange kinetics of ^{60}Co atoms among particulates, dissolved ions, and oxide layers formed on the surface of structural materials. First, it is assumed that particulates removed by the purification system have the same composition as particulates in the coolant leaving the core. Second, dissolved ions removed by the purification system will be replaced by particulates in the coolant entering the core. Third, the excess of released metal ions from the oxide layer is assumed to be transformed to particulates in the coolant. Finally, a certain amount of deposited metal ions from the coolant into the structural materials will be fillied up by the particulate present in the coolant. That is to say, some particulates will be dissolved into ions in order to compensate for the difference between solubility and the reduced ion concentration caused by the deposition into the oxide layer on the surface of structural materials. Under these assumptions, the relationship between n_{pi} and n_{po} for the case of positive temperature coefficient of solubility can be expressed from the out-core material balance as follows,

$$n_{po}\ C_{po} - \frac{P_{p,t}(t)}{F}\ n_{po} + \frac{R_t(t)-(1-k)\ D_i(t)}{F}\ n_d$$

$$- \frac{k\, D_i(t)}{F} \left(\frac{n_{po}+n_{pi}}{2} - n_d\right) - K_{po}\, C_{po}\, n_{po} - K_{pi}\, C_{pi}\, n_{pi}$$

$$+ \Delta C_d\, n_d = n_{pi}\, C_{pi} + \frac{P_{d,t}(t)}{F}\, n_{pi} \qquad \text{---------- (63)}$$

In the above equation, k represents the fraction of deposited metal ions which replaced by the dissolution of coolant particulates. The value of k will be evaluated later by using the experimental data which show the relationship between specific activity of dissolved ions and that of particulates in the coolant. Again, let's define g functions to simplify the solution to Eq. (63) as follows,

$$g_3 = \frac{F\, C_{pi}\, (1+K_{pi}) + P_{d,t}(t) + \frac{k}{2}\, D_i(t)}{F\, C_{po}\, (1-K_{po}) - P_{p,t}(t) - \frac{k}{2}\, D_i(t)} \qquad \text{---------- (64)}$$

$$g_4 = \frac{R_t(t) - (1-2k)\, D_i(t) + F\, \Delta C_d}{F\, C_{po}\, (1-K_{po}) - P_{p,t}(t) - \frac{k}{2}\, D_i(t)} \qquad \text{---------- (65)}$$

Then, Eq. (63) becomes

$$n_{po}(t) = g_3\, n_{pi}(t) - g_4\, n_d(t) \qquad \text{---------- (66)}$$

In the similar way, it is also possible to derive a differential equation for n_d from the above assumptions as follows,

$$\frac{d(n_d\, C_d\, W_C)}{dt} = P_{d,t}(t)\, (n_{pi} - n_d) + R_t(t)\, n_o(t)$$

$$- D_i(t)\, n_d + k\, D_i(t) \left(\frac{n_{po}+n_{pi}}{2} - n_d\right)$$

$$- \lambda\, n_d\, C_d\, W_C + \Delta C_d\, n_{po} \qquad \text{---------- (67)}$$

where W_C : total volume of primary coolant, m^3

Eq. (67) can be expressed as an ordinary first-order differential equation by assuming that every parameter except n_d is constant. This assumption is quite reasonable in the steady state. Therefore,

$$\frac{dn_d}{dt} = -\frac{(1+k)\ D_i(t) + P_{d,t}(t) + \lambda\ C_d\ W_C}{C_d\ W_C}\ n_d + \frac{\{P_{d,t}(t)+\frac{k}{2}D_i(t)\}n_{pi}+R_t(t)\,n_o(t)+(\frac{k}{2}D_i(t)+\Delta C_d)n_{po}}{C_d\ W_C} \quad (68)$$

The solution to Eq. (68) becomes

$$n_d(t) = g_5\ n_{pi}(t) + g_6\ n_o(t) + g_7\ n_{po}(t) \quad \text{---------- (69)}$$

In the above equation, g_5, g_6 and g_7 are defined as follows,

$$g_5 = \frac{P_{d,t}(t) + \frac{k}{2}\ D_i(t)}{(1+k)D_i(t) + P_{d,t}(t) + \lambda\ C_d\ W_C} \times \{1 - e^{-\frac{(1+k)D_i(t)+P_{d,t}(t)+\lambda\ C_dW_C}{C_d\ W_C}\ t}\} \quad \text{---------- (70)}$$

$$g_6 = \frac{R_t(t)}{(1+k)D_i(t) + P_{d,t}(t) + \lambda\ C_d\ W_C} \times \{1 - e^{-\frac{(1+k)D_i(t)+P_{d,t}(t)+\lambda\ C_dW_C}{C_d\ W_C}\ t}\} \quad \text{---------- (71)}$$

$$g_7 = \frac{\frac{k}{2}\ D_i(t) + \Delta C_d}{(1+k)D_i(t) + P_{d,t}(t) + \lambda\ C_d\ W_C} \times$$

$$\{1 - e^{-\frac{(1+k)D_i(t)+P_{d,i}(t)+\lambda C_d W_C}{C_d W_C} t}\} \qquad \text{---------- (72)}$$

From Eq. (43), the relationship between $n_o(t)$ and $n_d(t)$ for the hot leg side can be rearranged as follows,

$$n_o(t) = g_8\, n_d(t) + g_9\, n_{po}(t) \qquad \text{---------- (73)}$$

where g_8 and g_9 can be expressed as follows from Eq. (43).

$$g_8 = \frac{k_d\, C_d}{\{r_o\,(1+e)+\lambda\}\, W_o(t)} \left[1 - e^{-\{r_o\,(1+e)+\lambda\}\, t}\right]$$

$$= \frac{k_d\, C_d}{\{(1+e)+\frac{\lambda}{r_o}\}\,(k_c+k_d\, C_d+f\, k_d\, C_{po})} \times$$

$$\frac{\{1 - e^{-\{r_o\,(1+e)+\lambda\}\, t}\}}{(1 - e^{-r_o t})} \qquad \text{---------- (74)}$$

$$g_9 = \frac{f\, k_d\, C_{po}}{\{(1+e)+\frac{\lambda}{r_o}\}\,(k_c+k_d\, C_d+f\, k_d\, C_{po})} \times$$

$$\frac{\{1 - e^{-\{r_o\,(1+e)+\lambda\}\, t}\}}{(1 - e^{-r_o t})} \qquad \text{---------- (75)}$$

Now, $n_d(t)$, $n_{pi}(t)$, $n_{po}(t)$ and $n_o(t)$ can be solved from Eq. (49), (66), (69) and (73). They are obtained as follows,

$$n_d(t) = \frac{g_2\,(g_5+g_3\, g_6\, g_9)}{(g_3-g_1)\,(1-g_6\, g_8+_4\, g_6\, g_9)-g_4\,(g_5+g_3\, g_6\, g_9)} \qquad (76)$$

$$n_{pi}(t) = \frac{1-g_6\, g_8+g_4\, g_6\, g_9}{g_5+g_3\, g_6\, g_9}\, n_d(t) \qquad \text{---------- (77)}$$

$$n_{po}(t) = \frac{g_1(1-g_6\ g_8+g_4\ g_6\ g_9)}{g_5+g_3\ g_6\ g_9}\ n_d(t) + g_2 \qquad \text{---------- (78)}$$

$$n_o(t) = \{\frac{g_1\ g_9\ (1-g_6\ g_8+g_4\ g_6\ g_9)}{g_5+g_3\ g_6\ g_9} + g_8\ \}\ n_d(t) + g_2\ g_9 \qquad (79)$$

From Eq. (37) and (79), total ^{60}Co activity deposited on structural materials can be evaluated. In chapter 6, the inventory of ^{60}Co will be analyzed by using EXCEL worksheet.

6. EVALUATION OF ^{60}Co INVENTORY

6-1 Parameters for the Evaluation

Parameters related to the structural materials for the evaluation of the ^{60}Co inventory deposited in the primary coolant system of PWRs are summarized in Table 6-1. These data constitute the basic information used to calculate transport kinetics of crud in the primary coolant system. In this table, the surface area was taken from the data for the Trojan NPP that appeared in Ref. 16. The surface area enduring wear was adjusted to give the cobalt input from the wear rate adopted in this report, because it was not focussed on the evaluation of cobalt sources. There is no data available to evaluate the deposition of crud from the coolant onto the isothermal surface of Inconel-600, so the same deposition rate constant as that onto the S/G tubing was assumed. Even though there must be some differences in the corrosion rate, release rate, and deposition rate between in-core structural materials and out-core structural materials due to the difference of temperature, the rate constants are assumed to remain constant. However, the concentration of dissolved metal ions will be adjusted for each region according to the change of solubility in the coolant.

Table 6-2 provides some key parameters regarding the primary coolant system for a typical 4-loop PWR. The chemical volume control system (CVCS) will be considered the only purification system in the primary coolant circuit. Decontamination factors in the CVCS are assumed as 10 for particulates, and 100 for dissolved ions. As shown in the table, the CVCS flow rate is less than 0.03% of the total coolant flow rate passing through the core.

Some parameters needed for the evaluation of in-core activation of ^{59}Co are given in Table 6-3. Epithermal absorption cross section of ^{59}Co estimated in Ref. 10 by considering the thermal-to-epithermal neutron ratio in the Point Beach NPP was used here.

Table 6-1

Assumed Paramaters for Structural Materials
Used in a Typical Westinghouse PWR

Structural Material	Cobalt Content	Corrosion/Wear Rate Constant ($g/m^2 \cdot s$)	Release Rate Constant (s^{-1})	Cobalt Enrichment Factor	Deposition Rate Constant (m/s)	Surface Area[a] (m^2)
S/S 304	2×10^{-3}	7.716×10^{-8}	4.16×10^{-7}	0.67	8.53×10^{-4}	1,603(Core) 555(Fuel) 138(Hot)[b] 479(Cold)[b] 186(HX)
Inconel-600 (S/G Tubes)	5×10^{-4}	1.929×10^{-7}	5.56×10^{-8}	1.37	2.28×10^{-6}	17,929
Inconel-600 (Others)	5×10^{-4}	1.929×10^{-7}	5.56×10^{-8}	1.37	2.28×10^{-6}	32(Core) 728(Fuel)
Stellite-6 (Corrosion)	0.55	1.929×10^{-7}	1.0	-	-	9.23
Stellite-6 (Wear)	0.55	1.929×10^{-6}	1.0	-	-	0.28
Zircaloy Cladding	-	-	1.83×10^{-6}	-	7.94×10^{-4}	7,234

Note) a. The surface area was evaluated based on Ref. 16.

b. Hot means the structural materials which compose the hot leg of primary coolant circuit. Cold means the structural materials which compose the cold leg of primary coolant circuit including pressurizers and reactor coolant pumps.

Table 6-2

Assumed Parameters for a Typical PWR Primary Coolant System

Primary Coolant Flow Rate		18.0 m^3/s
Core Inlet Temperature		292 ℃
Core Outlet Temperature		327 ℃
CVCS Flow Rate		4.7×10^{-3} m^3/s
CVCS Decontamination Factor	Dissolved Metal Ions	100
	Particulates	10

Table 6-3

Assumed Parameters Related to the Neutron Activation of ^{59}Co[10)]

Reaction Cross Sections for $^{59}Co(n,\gamma)^{60}Co$, $(cm^2\times10^{24})$	σ_{th}	37.2
	σ_{epth}[a]	32.8
Thermal Neutron Flux, $(neutrons/m^2\cdot s)$[b]		2.0×10^{18}

a. Epithermal cross section given in Ref. 10 has been adjusted by the ratio of epithermal-to-thermal neutrons.

b. Thermal neutron flux was assumed from the residence time evaluated in the reference.

6-2 Modeling the Effect of Refueling

A certain amount of crud deposited on the fuel rod is removed permanently from the primary coolant system by refueling. In order to reflect the crud removal in the outage period, one-third refueling per year will be assumed.

Some equations relating to fuel deposition should be modified to model the effect of refueling on the crud transport mechanism. The amount of fuel deposit should be obtained for the every core region. For example, Eq. (18) should be modified as follows,

$$W_{F,j} = \frac{k_f C_{pi}}{r_f} (1 - e^{-r_f T_j}) \quad \text{---------- (80)}$$

where $W_{F,j}$: the amount of crud deposited on the fuel rod in the j region

T_j : the time elapsed after loading the fuel in the j region (no more than three years)

Besides the amount of fuel deposit, the number of ^{60}Co atoms per gram deposit(n_f) as metal components should be also modified. In Eq. (49), n_f of the deposit formed on the fuel rod, which belongs to the region j, can be simply adjusted by replacing t with T_j.

The concentration of particulates in the coolant must be affected by the reduced release rate of particulates from the fuel rod into the coolant. Therefore, $f_1(t)$ in Eq. (57) and (58) should be modified as follows,

$$f_1(t) = 1 - \frac{A k_f}{3F} (e^{-r_f T_1} + e^{-r_f T_2} + e^{-r_f T_3}) \quad \text{------- (81)}$$

where the relationship between t and T is

$$t = T_1 = T_2 = T_3 \quad \text{if } t < 1 \text{ yr } (3.15\times10^7 \text{ sec})$$

$$t = T_2 = T_3 = T_1 + 3.154\times10^7 \quad \text{if } 1 \text{ yr} \le t < 2 \text{ yrs}$$

$$t = T_1 + m \times 3.154\times10^7$$

$$= T_2 + (m - 1) \times 3.154\times10^7$$

$$= T_2 + (m - 2) \times 3.154\times10^7 \quad \text{if } m(\ge 2) \text{ yrs} \le t < (m+1) \text{ yrs}$$

Because the other quantities are subject to the changes of W_F, n_f, C_{po}, C_{pi}, it is possible to evaluate them without modifying the equations.

6-3 ^{60}Co Inventory in the PWR Primary Coolant System

In order to evaluate the ^{60}Co inventory accumulating in the primary coolant system of a PWR, a simple computer program based on an EXCEL spreadsheet was prepared. In this program, the solubility data of nonstoichiometric nickel ferrite in high-temperature aqueous solution measured by Y. L. Slandler and R. H. Kunig were used to calculate the steady-state concentration of metal ions present in the coolant. Then the concentration of particulates in the coolant was evaluated by using Eq. (59) and (60). Based on the evaluated concentrations of particulates and metal ions in the colant, the thickness of deposits forming on the surface of structural materials was calculated from Eq. (18) and (37). The structural materials were classified as to alloy types and installed positions, such as hot leg side or cold leg side. The specific activities of ^{60}Co in the crud present in the coolant and in the deposit accumulated on the structural materials were evaluated by using Eq. (50), (76), (77), (78), and (79). Finally, the inventory of ^{60}Co accumulating in the primary coolant system was evaluated from the thickness of deposit and the specific activity.

Fig. 6-1 shows the concentration of coolant particulates in the coolant. From this graph, it is shown that the concentration of coolant particulates will reach the equilibrium value of 9.94×10^{-3} g/m^3 in the coolant entering the core, and 8.92×10^{-3} g/m^3 in the coolant leaving the core. The difference between the concentration in the coolant entering the core and that in the coolant leaving the core reflects the change in the solubility in the steady state. In order to calculate the concentration of coolant particulates, the fraction of particulate deposition was evaluated to meet the range of particulate concentrations found in in-reactor loop experiments. The estimated value of f 0.161 was used in this report. The concentration of particulates in the coolant is strongly dependent on the total release rate into the coolant, total deposition rate on structural materials, water chemistry, purification system, coolant flow rate, etc. It means the particulate concentration varies from plant to plant depending on the types of structural materials, surface area contacting with coolant, etc. However, the data from some experiments were used here to evaluate the value of f. Particulate deposition rate constants estimated

from ionic deposition rate constants and f are as follows :

$$k_{pd} = f\, k_d = 1.37\times10^{-4} \quad m/s \quad \text{for stainless steel}$$

$$k_{pd} = 3.67\times10^{-7} \quad m/s \quad \text{for Inconel-600}$$

The concentration of particulates obtained here is somewhat higher than the concentration found in Doel 3 and 4 ($2.81\times10^{-4}\sim1.58\times10^{-3}$ g/m^3). However, some measured data of ^{60}Co activity in the coolant of Kori #1 suggest higher particulate concentration than these results. This observation will be discussed later. From these results, it should be noted that the particulate deposition from the coolant into oxide layer is very important in the analysis of crud transport in the primary coolant system, even though ionic deposition is dominant compared to the particulate deposition.

The thickness of deposit forming on the surface of structural materials is shown in Fig. 6-2. From this figure, the following findings can be noted:

- The thickness of deposits forming on the surface of structural materials reaches a steady state value after three cycles' operation. It implies that the increase in the release rate of metal ions from oxides into the coolant balances the deposition and corrosion rates.
- The deposit formed on stainless steel used in the hot leg side is about 14 % thicker than that formed on stainless steel used in the cold leg side. If there is no particulate deposition, the deposit formed on stainless steel in the hot laeg side must be much thicker than that formed on stainless steel used in the cold leg side. However, increased deposition of particulates in the cold leg side makes the difference of deposit thicknesses between in the hot leg side and in the cold leg side negligible. If we can find some real data from operating plants, the contribution of particulate deposition can be analyzed more exactly by using the method suggested here.
- The thickness of deposit formed on Inconel-600 has reached its steady state value of 3.7 g/m^2. No discernable difference in the deposit thicknesses was

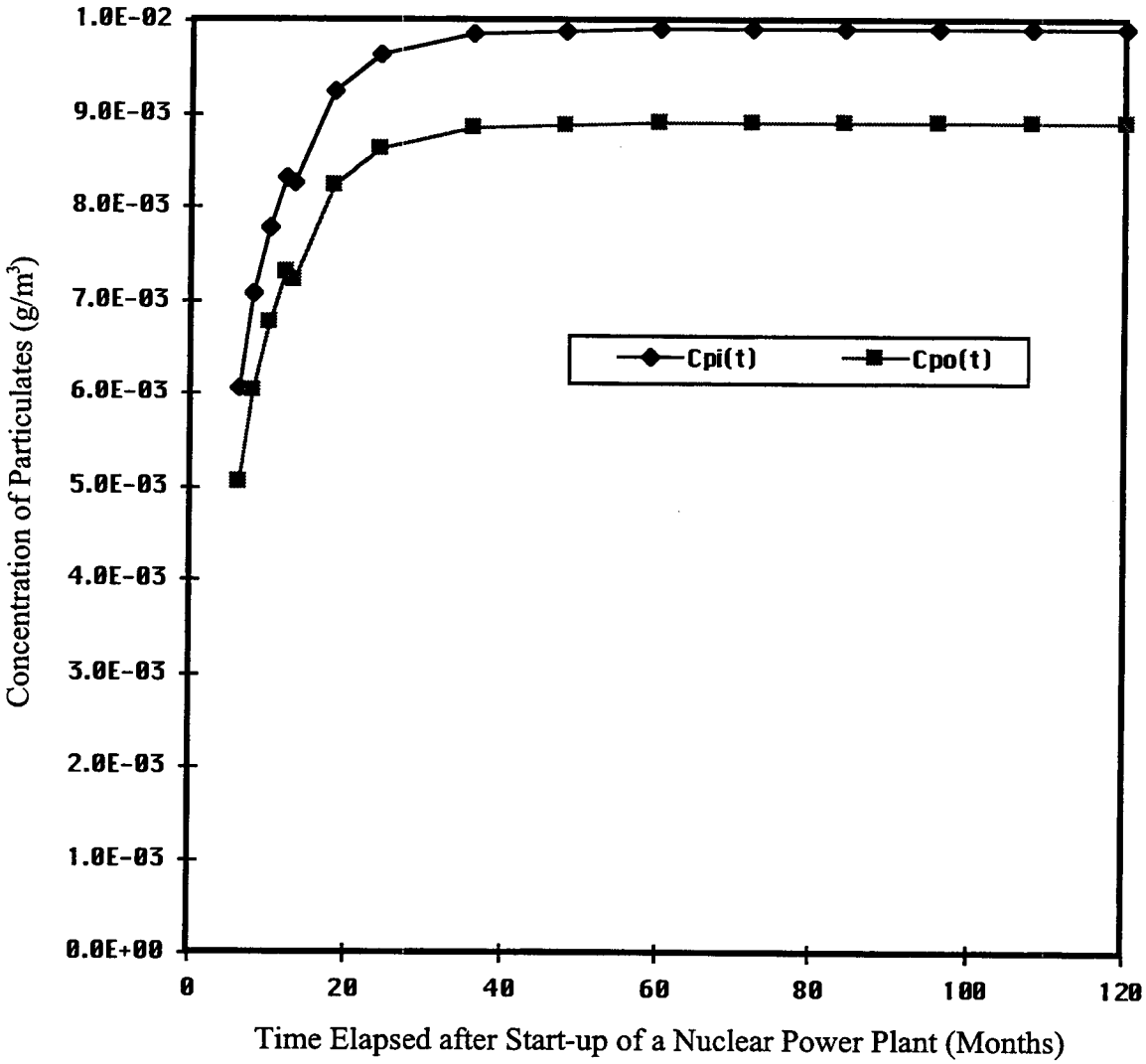

Figure 6-1 Concentration of Particulates as Metal Components in the Coolant (Cpi : Concentration of Particulates in the Coolant Entering the Core; Cpo : Concentration of Particulates in the Coolant Leaving the Core)

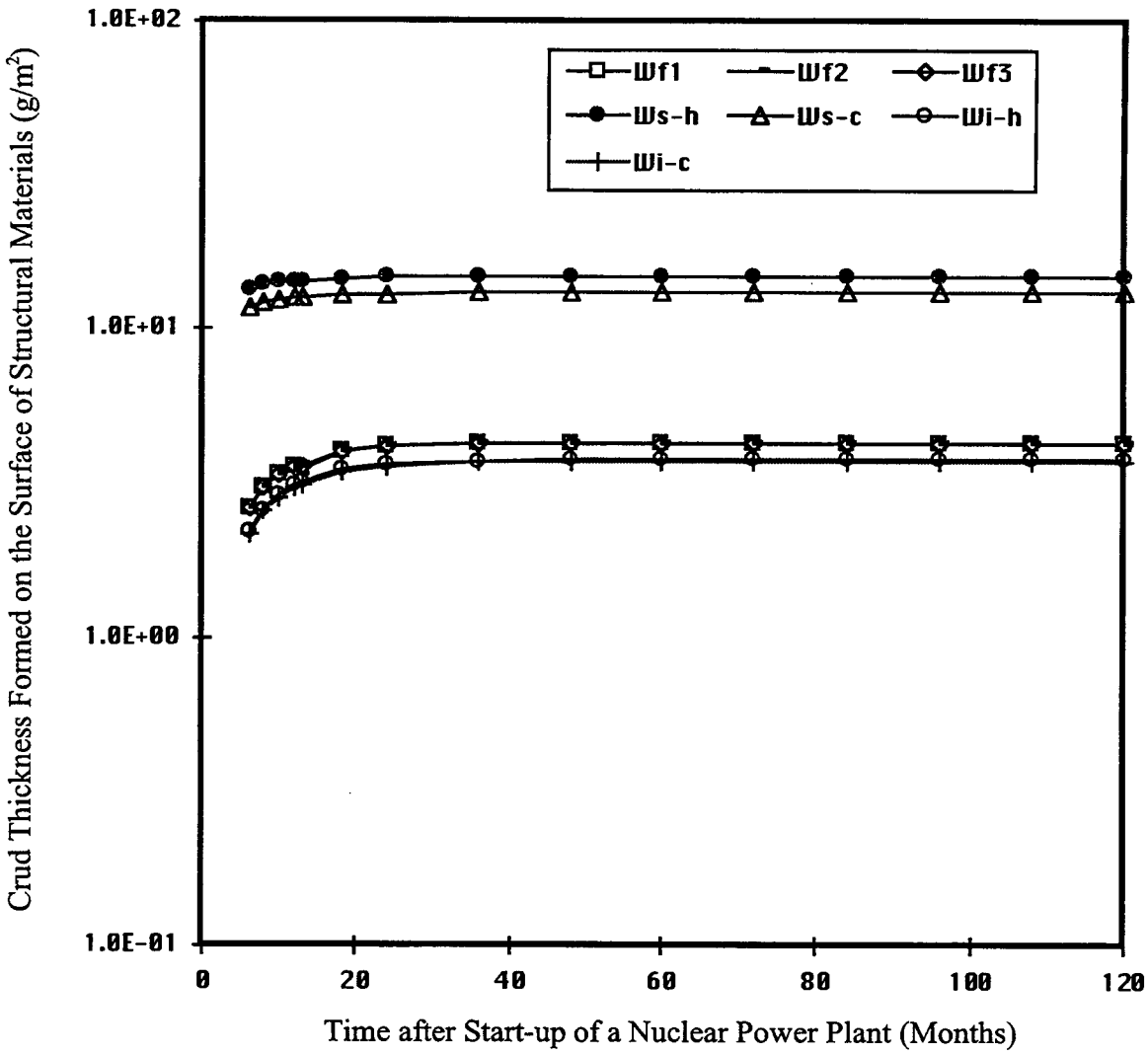

Figure 6-2 Crud Thickness Forming on the Surface of Structural Materials (Wf1, Wf2, Wf3 : Thickness of Fuel Deposit; Ws-h, Ws-c : Thickness of Oxides(as Metal Components) Formed on the Surface of S/S 304; Wi-h, Wi-c : Thickness of Oxides(as Metal Components) Formed on the Surface of Inconel-600; h and c Designate the Hot Leg and Cold Leg, Respectively)

observed between the hot leg side and the cold leg side. This must be because of the low deposition rate of metal ions and particulates from the coolant being incorporated into the oxide layer formed on Inconel-600.

- The steady state thickness of crud deposited on fuel rods is approximately 4.3 g/m^2 (1.0 mg/dm^2), which is a little bit higher than the thickness of fuel deposit (0.03~2.02 g/m^2) of fuel deposit thickness found in the WEP cycle 1 core. However, it showed a good agreement with the deposit thickness (3.3~ 33 g/m^2) found in NOK cores.

It is not easy to compare the thickness of deposit formed on structural materials with the deposit data found in the operating nuclear power plant because of the lack of information. However, the thickness formed on fuel rod suggests that the model developed in this report is suitable for the analysis of crud deposition in the primary coolant system of a PWR.

Fig. 6-3 shows the specific activity of ^{60}Co of crud present in the coolant and the deposits formed on structural materials. In order to calculate the specific activity, the fraction of deposited metal ions from the coolant into oxide layer, which is replaced by the dissolution of coolant particulates, was evaluated based on the ratio between specific activity of dissolved species and that of particulates in the coolant. The ratio in the steady state was assumed to be 0.28 from the experimental results by P. V. Balakrishnan and G. M. Allison.[7] The fraction(k) was adjusted to give the desired value (0.28) of the ratio, and the value of 0.85 was selected as the fraction in this model. It means 85 % of metal ions incorporated into the oxide layer formed on structural materials will be replaced by the dissolved metal ions from particulates present in the coolant. By using this concept, it is also possible to explain exchange reation of cobalt between dissolved metal ions and particulates in the coolant. Also the exchange reaction results in higher concentration of ^{60}Co in the dissolved species than expected. The following features can be emphasized from the graph.

- Unlike the deposit thickness, the specific activity of crud shows a small decrease after refueling. This is caused by the pick-up of particulates released from old fuel, which contains high ^{60}Co atoms, by new fuel.

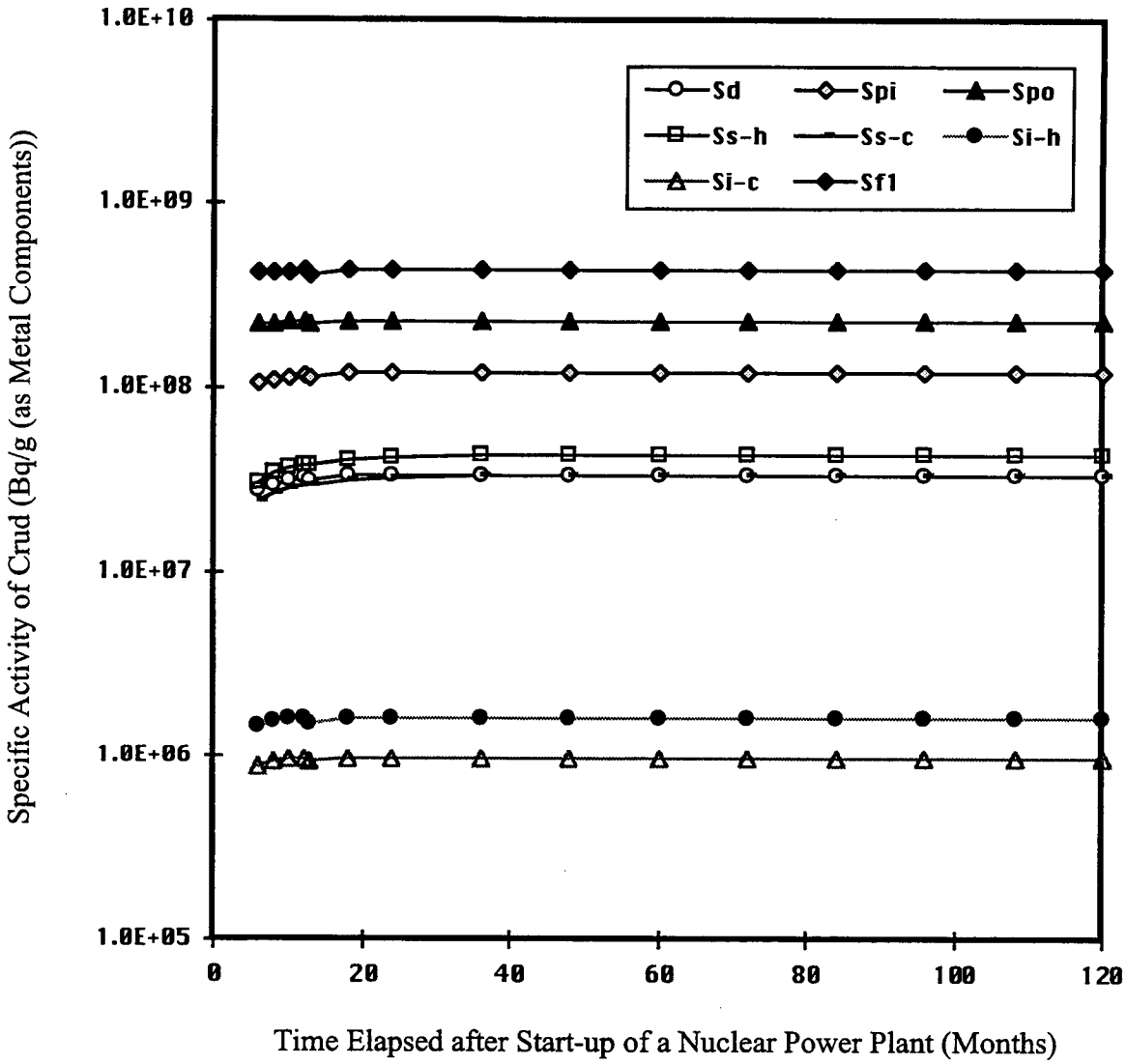

Figure 6-3 The specific Activity of ^{60}Co present in Crud (d: Metal Ions in the Coolant; pi: Particulates in the Coolant Entering the Core; po: Particulates in the Coolant Leaving the Core; s-h: Stainless Steel in the Hot Leg; s-c: Stainless Steel in the Cold Leg; i-h: Inconel-600 in the Hot Leg; i-c: Inconel-600 in the Cold Leg; f1: Fuel in the Region 1)

- The specific activity of particulates increases about two times while going through the core, although there is no discernable change in the concentration of particulates. This reflects the rapid exchange reaction of particulates between the deposits on fuel and the coolant. This big difference in the specific activity of particulates in the coolant entering and leaving the core can be explained as a force which drives the activation of out-core primary coolant system.

- The specific activity of the oxide layer forming on stainless steel shows a 30 % higher level in the hot leg than in the cold leg. However, the specific activity of oxide layer formed on Inconel-600 in the hot leg side reveals a 60 % higher value than that in the cold leg side. It implies that particulate deposition is much more dominant in the hot leg side and Inconel-600 compared to the cold leg side and stainless steel.

- The specific activity of oxide layer forming on stainless steel is much higher (more than 25 times) than that of oxide layer formed on Inconel-600. This difference makes a primary coolant piping made of stainless steel as an important radiation source.

- Most important is the fact that the specific activity of the oxide layer forming on stainless steel in the hot leg side is about 25 % higher than that of dissolved metal ions in the coolant. If there is no particulate deposition onto the oxide layer, the specific activity of dissolved metal ions must be higher than that of the oxide layer in any case. This is also consistent with findings from in-reactor loop experiments, which shows higher specific activity in the pipe section deposit than in the dissolved species.[7)]

The inventory of ^{60}Co accumulated on the primary coolant system, which is obtained by multiplying the thickness of oxide layer and the specific activity, is shown in Fig. 6-4. In this graph, the following findings can be noted:

- Accumulation of ^{60}Co atoms in the oxide layer formed on stainless steel is the most important sink for the ^{60}Co inventory in the primary coolant system of a PWR. In this model, stainless steel used in heat exchangers was treated the same as stainless steel used in cold leg side. That is why the inventory of

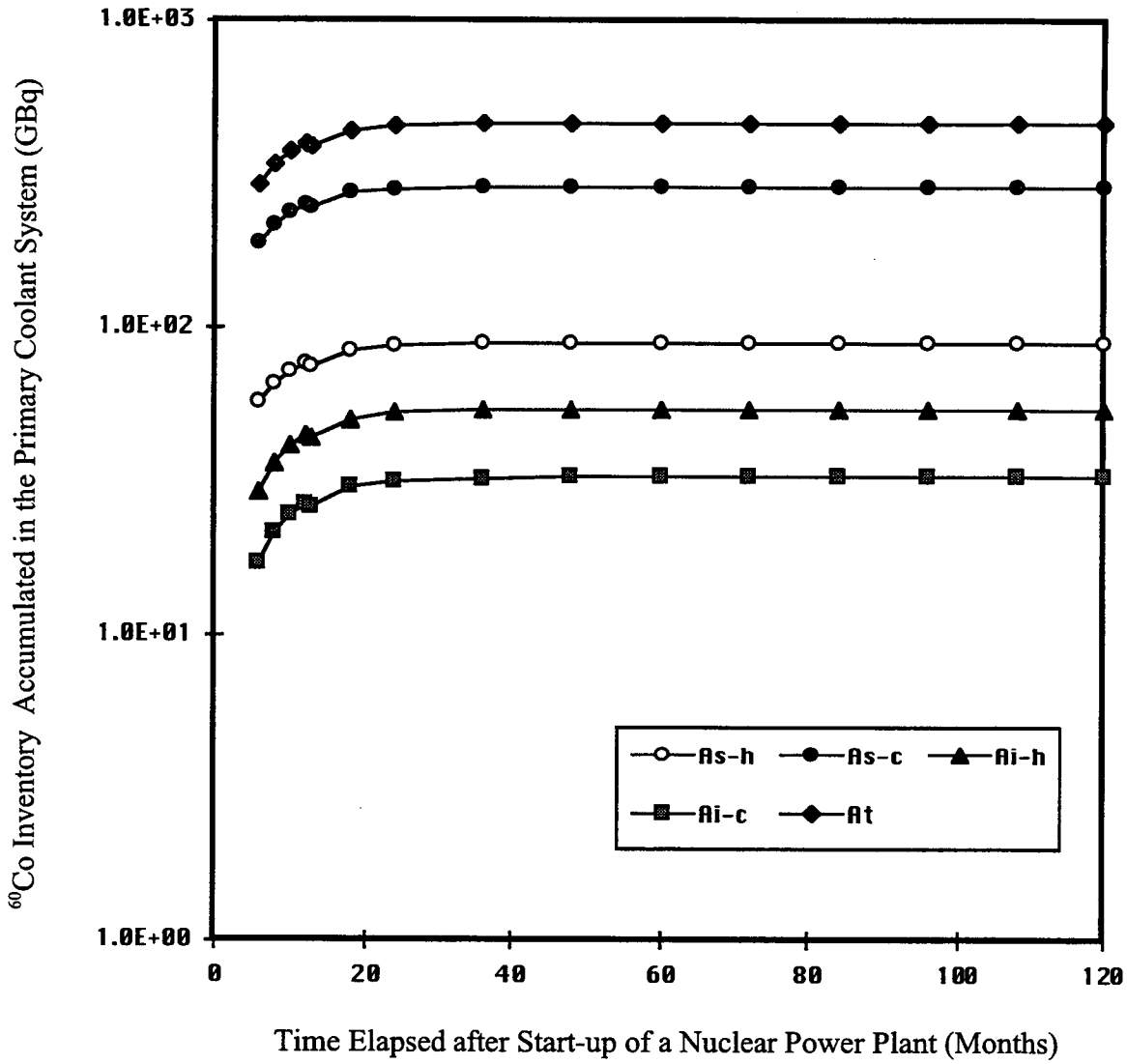

Figure 6-4 The inventory of ^{60}Co Accumulated in the Primary Coolant System (s-h: Stainless Steel in the Hot Leg; s-c: Stainless Steel in the Cold Leg; i-h: Inconel-600 in the Hot Leg; i-c: Inconel-600 in the Cold Leg; t: Total)

^{60}Co accumulating on stainless steel used in the cold leg side is about 62 % of the total inventory. There must be some difference in the processes of corrosion, release, and deposition depending on the environment such as water chemistry, temperature, etc. However, it is impossible to get enough data to incorporate the difference in the model used here.

- Even though the area of Inconel-600 is much larger than that of stainless steel, the total inventory of ^{60}Co picked up by oxide layer forming on Inconel-600 is about the same as the inventory ^{60}Co in the oxide layer forming on stainless steel used in the hot leg side due to the smaller thickness and lower specific activity of the oxide layer forming on Inconel-600.

- No increase in the total inventory is anticipated after three cycles' operation. Table 6-14 shows the inventory of ^{60}Co deposited on out-core components in the equlibrium state, which is evaluated from the relative surface area of structural materials used in each component and from the inventory of ^{60}Co picked up by the relevant material. The data given in Table 6-1 can be used to evaluate dose rates from each component by considering the geometry of each component.

Fig. 6-5 shows the contamination level of ^{60}Co activity deposited in the primary coolant system. It is concluded that the contamination level of ^{60}Co on the surface of stainless steel can reach up to 5.2 $\mu Ci/cm^2$ from the figure. The contamination level of ^{60}Co on stainless steel shows a value about 100 times higher than that on Inconel-600. Therefore, careful attention should be paid to maintenance work on components that are made of stainless steel parts, such as main coolant pumps. However, the contamination level evaluated for steam generator tubes seems quite low compared to the contamination level found in several Westinghouse-designed PWRs. This may be explained by differences in water chemistry. Because the solubility increases at low pH, and the temperature coefficient of solubility becomes negative, lower pH than 7.4, which is used here to analyze ^{60}Co contamination level, causes thicker deposits and higher specific activity than the values obtained in this report.

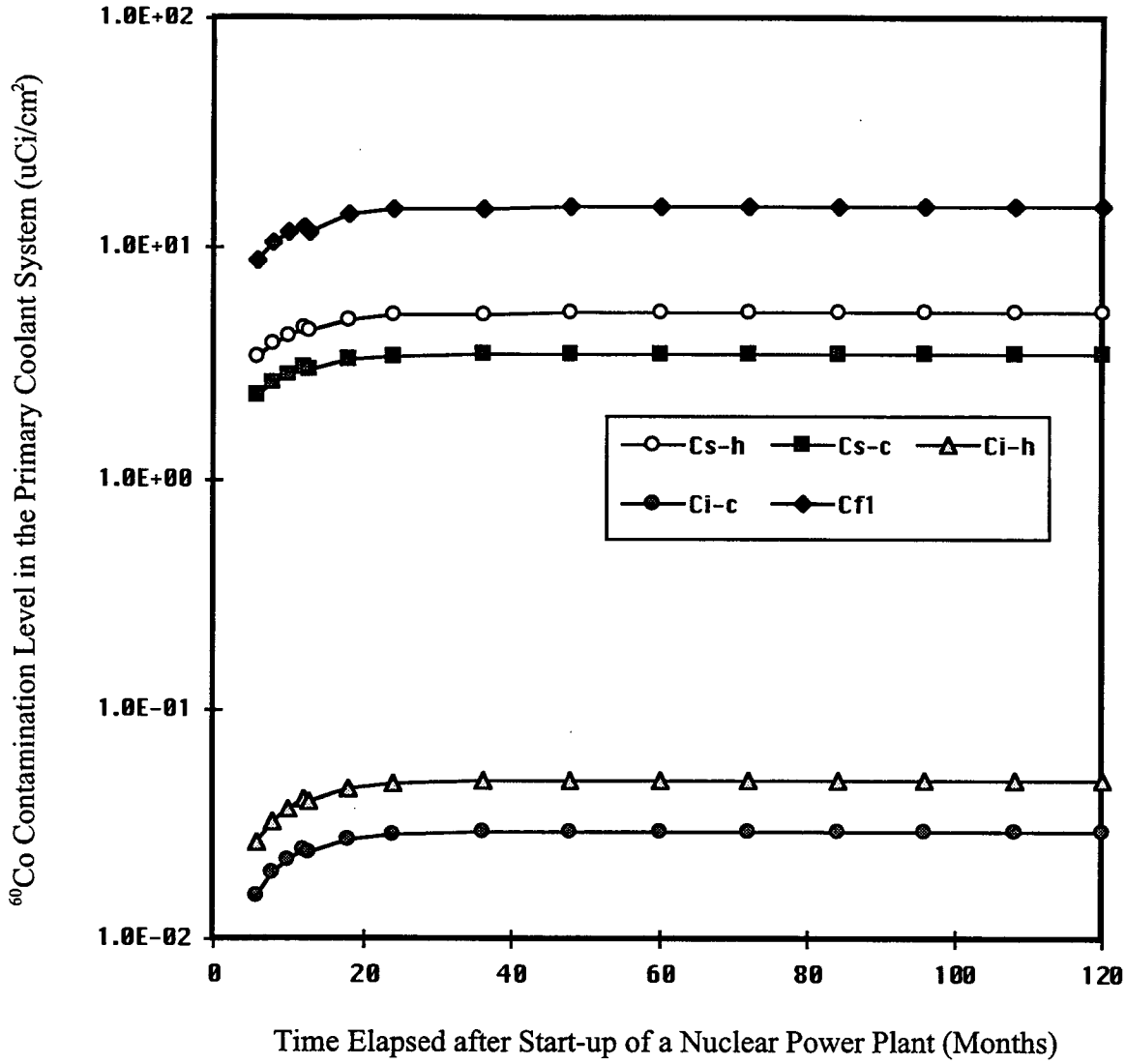

Figure 6-5 ^{60}Co Activity Level Accumulated in the Primary Coolant System (s-h: Stainless Steel in the Hot Leg; s-c: Stainless Steel in the Cold Leg; i-h: Inconel-600 in the Hot Leg; i-c: Inconel-600 in the Cold Leg; f1: Fuel Region 1)

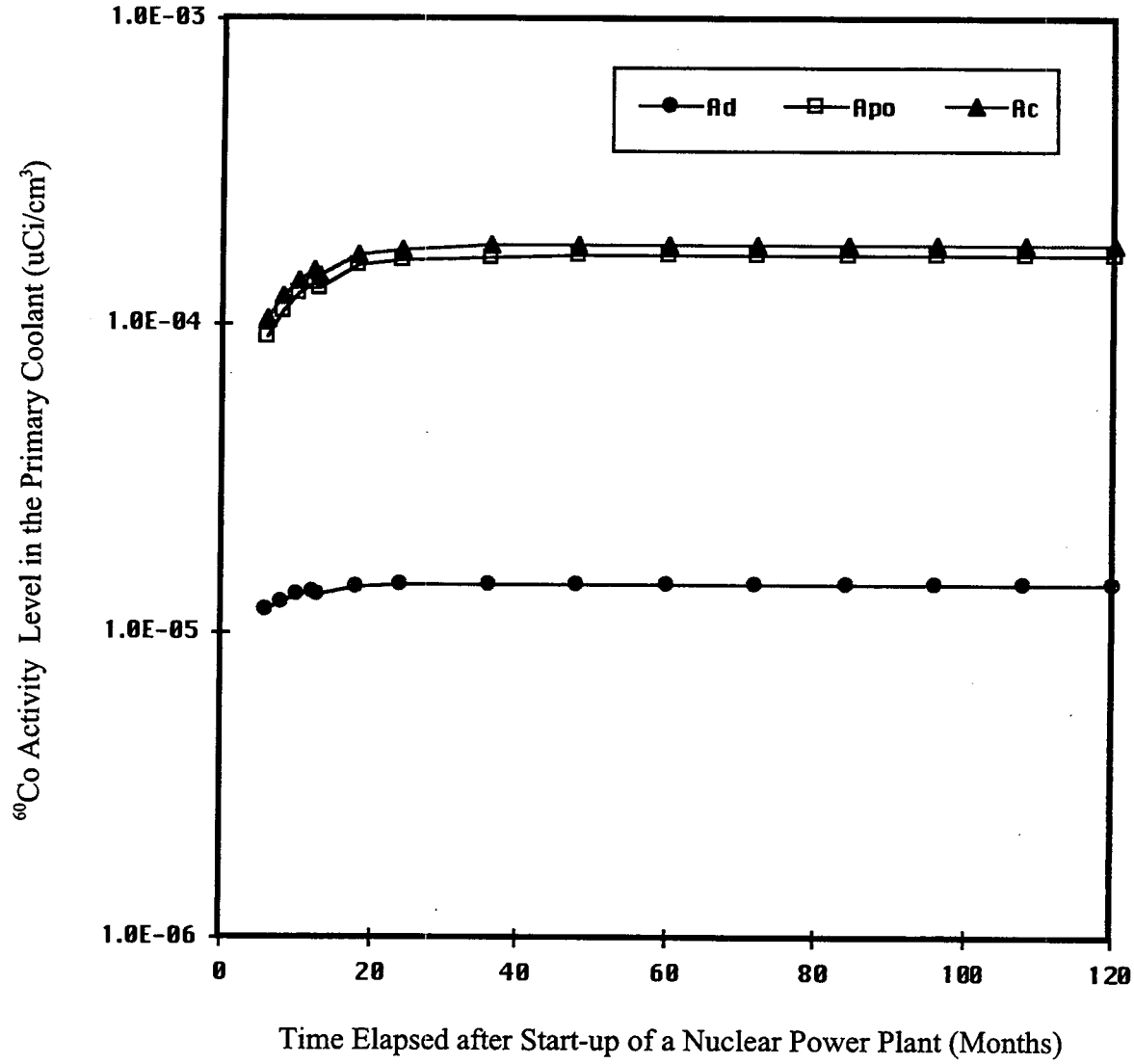

Figure 6-6 ^{60}Co Activity Level in the Primary Coolant (d: Dissolved Metal Ions; po: Particulates in the Hot Leg Side; t: Total)

Table 6-14

The inventory of ^{60}Co Deposited on Out-Core Components

(Unit : GBq)

		Hot Leg Side	Cold Leg Side	Total
Steam Generator	Tubes	54.2	32.7	86.9
	Chamber	22.5	15.3	37.8
	Sub-Total	76.7	48.0	124.7
Main Coolant Piping		66.3	44.9	111.2
Pressurizer			54.9	54.9
Main Coolant Pump			93.8	93.8
Heat Exchangers			81.1	81.1
Total		143.0	322.7	465.7

Fig 6-6 shows the level of ^{60}Co activity in the coolant. The results show good consistency with the measured values from in-reactor experiments, although the total activity of ^{60}Co in the coolant shows somewhat lower level than the values reported from Kori-1. It is interesting that most of activity of ^{60}Co in the coolant comes from particulates. We can postulate that the concentration of dissolved metal ions in the coolant is less than the solubility of parent metal oxides. And the specific activities of ^{60}Co in the dissolved species and particulates in the coolant cannot exceed certain levels which are limited by the activation rate of ^{59}Co in the core. Therefore, the increase in the level of ^{60}Co in the coolant can be used to

anticipate the concentration of particulates present in the coolant. If, for example, the ^{60}Co activity in the coolant is higher than 1.8 $\mu Ci/cm^3$ in a certain nuclear power plant, it implies that the concentration of particulates in the coolant must be higher than the value evaluated in this report. There are several factors which affect the concentration of particulates in the coolant.

- The ratio between the surface area of Inconel-600 and that of stainless steel is the key parameter which decides the concentration of coolant particulates. Inconel-600 is the main source of crud which accumulates in the primary coolant system, because it shows a high corrosion rate and a low deposition rate. Even though the release rate of metal oxides from Inconel-600 is lower than that of metal oxides from stainless steel, most of the corrosion products from Inconel-600 are released into the coolant. The higher the ratio is, therefore, the higher the concentration of coolant particulates.

- The removal rate of particulates from the coolant is also important. If the flow rate to CVCS is increased, the concentration of particulates in the coolant will decrease. The effect can be easily analyzed by using the model developed here.

- Water chemistry may affect the deposition process. For example, the rate of particulate deposition can be strongly controlled by the water chemistry. In fact, some experimental results show the large variation in the concentration of coolant particulates depending on the coolant chemistry condition. It is not easy to decide the effect of water chemistry at this moment. Besides, water chemistry certainly affect the solubility of nickel ferrite in the coolant. High solubility suppresses the concentration of particulates in the coolant, and low solubility increases the concentration of particulates. In chapter 5, we suggested a method to reflect the effect of water chemistry. However, a detail analysis will be reserved for future study.

The concentration of particulates in the coolant appears to be the most important parameter which reflects the characteristics of crud transport in the primary coolant system. The thickness of the deposit, the ^{60}Co concentration in the deposit, and the total inventory of ^{60}Co in the primary coolant system depend on the concentration of particulates in the coolant. (See equations developed in chapter 5.) For example,

if there is any change in the environment which results in the increase of particulate concentration in the coolant, it is clear that the total inventory of ^{60}Co increases from the equations developed in chapter 5. Therefore, the level of ^{60}Co activity in the coolant can be interpreted as the level of ^{60}Co inventory in the primary coolant system.

It is very convenient to use the model developed here in order to predict the ^{60}Co inventory in the primary coolant system from design data, such as surface area of structural materials, in-core neutron flux, primary coolant condition, purification system, etc. However, it should be noted that there are some limitations on its use.

- Some parameters were derived on the basis of steady state in order to solve the non-linear differential equation analytically. Therefore, this model cannot be used to predict the deposition of cobalt in the transient state, such as startup and refueling.
- In order to explain the low concentration of particulates in the coolant, particulate deposition was assumed in this model. Even though the results showed good agreement with findings from in-reactor experiments, it is doubtful to use the fraction of particulate deposition estimated from this model in any situation.
- The surface conditions of structural materials and flow conditions are not considered in this model. Therefore, it is impossible to analyze particulate traps, which can cause the local accumulation of activity.

7. CONCLUSIONS

By reviewing the previous work regarding corrosion behavior of structural materials used in PWRs, linear kinetics was selected to evaluate the cobalt input from the structural materials into the coolant by corrosion. It is evident that the corrosion kinetics of metals is controlled by the diffusion of ions through the pores present in the oxide film. Therefore, it is more logical to assume that corrosion kinetics follows the parabolic expression in a closed high temperature system like the PWR primary coolant circuit. However, a conservative approach was adopted for predicting the long-term behavior of a PWR, because the nuclear primary coolant system is not a closed system at all.

Radiochemical analysis results show the possibility of ionic release kinetics of metal oxides from oxide films formed on structural materials into the coolant. The release rate of metal oxides from oxide films into the coolant was assumed to be proportional to the thickness of oxide films. Experimental results reported in the previous work were used to evaluate release rate constants for stainless steel and Inconel-600. The release rate constants are $4.16\times10^{-7}\ s^{-1}$ for stainless steel, and $5.56\times10^{-8}\ s^{-1}$ for Inconel-600. In this report, selective release of ions was assumed. For example, cobalt ions are assumed to be enriched 137 % in the aqueous solution compared to the oxide films formed on Inconel-600.

It is certain that deposition kinetics from the coolant onto fuel rods is controlled by particulate deposition based on previous work. The release kinetics from fuel deposits into the coolant seems to be controlled by the release rate of particulates due to erosion from the surface of deposit. In this case, the release rate is affected by the thickness of the loosely-attached layer. To develop an analytical solution, however, the fuel deposit was assumed to be a loosely-attached layer. The measured data from the WEP core and the in-reactor loop experimental results of Balakrishnan and Alison were used to evaluate the deposition rate constant of coolant particulates onto fuel rods and the erosion rate constant of fuel deposits into the coolant. In order to evaluate the rate constants, an equation for neutron

activation of ^{59}Co was derived. The rate constants obtained here are 7.94×10^{-4} m/s for deposition kinetics, and 1.83×10^{-6} s^{-1} for release kinetics.

The incorporation of activated corrosion products from the coolant into the oxide films formed on structural amterials seems to be controlled mostly by ionic deposition kinetics. By assuming the ionic deposition kinetics, therefore, deposition rate constants were evaluated by using the concept of equilibrium oxide thicknesses, which were calculated from Lister's mathematical expressions for the oxide growth rate on structural materials. The estimated values are 8.53×10^{-4} m/s for stainless steel, and 2.28×10^{-5} m/s for Inconel-600. However, the possibility of particulate deposition from the coolant into the oxide films was also considered in order to explain why the specific activity of pipe section deposits is higher than that of dissolved ions in the coolant found in in-reactor experiments, and why the particulate concentration in the coolant is lower than the expected level from the ionic deposition model. The fraction of partculate deposition was evaluated based on the concentration of particulates in the coolant. In order to evaluate the ^{60}Co inventory deposited on the primary coolant system, mathematical expressions for the thickness of oxide films formed on structural materials, and the specific activity of the oxide films were derived based on the above-mentoned transport kinetics of corrosion products in the PWR primary coolant system.

An EXCEL spreadsheet was used to calculate total ^{60}Co inventory in the primary coolant system. The results showed that the thickness of deposit has reached its steady-state value only after three cycles of operation. The thickness of oxide films formed on stainless steel in the hot leg side was 14.9 g/m^2 in the steady state. The thickness of oxide films formed on Inconel-600 was about one-fourth of that formed on stainless steel. The difference in the thicknesses of oxide films formed in the hot leg side and the cold leg side depended on the type of structural material. For example, stainless steel showed more than 10 % increase in the hot leg side, however, no appreciable difference was shown in the case of Inconel-600.

Oxide films formed on stainless steel in the hot leg side showed the highest specific activity of 4.33×10^{7} Bq/g, which is even higher than that of dissolved ions in the coolant. This result showed good agreement with results from in-reactor

loop experiments. The lowest specific activity in the oxide films formed on structural materials was found in Inconel-600 used in the cold leg side, and it was 9.77×10^5 Bq/g in the steady state. The specific activity of particulates in the coolant showed a considerable difference between those entering the core and leaving the core.

A predicted value of the total inventory of ^{60}Co in the out-core primary coolant system was 466 GBq; 143 GBq in the hot leg side, and 323 GBq in the cold leg side. The most important radiation sources in the out-core primary coolant system are main coolant pumps.

The contamination level of ^{60}Co in the deposit was also evaluated. The highest contamination level of 5.22 $\mu Ci/cm^2$ was anticipated in the deposit forming on stainless steel in the hot leg side. However, the contamination level of oxide films forming on Inconel-600 showed values about 100 times lower level than those of oxide films forming on stainless steel. It is interesting that most of ^{60}Co radioactivity in the coolant comes from particulates. Therefore, ^{60}Co activity in the coolant can be used as a measure for predicting the concentration of particulates in the coolant.

The model developed here can be used to explain some findings from in-reactor experiments and field measurements. The model is very simple and is very easy to modify. Therefore, it is very convenient to use the model for predicting ^{60}Co inventory, contamination level, and coolant activity. However, it is not appropriate to use this model in order to analyze transient state, extremely low or high pH conditions, and particulate trapping.

8. REFERENCES

1. N. K. Taylor, "Review of Available Data on the Release, Transport and Deposition of Corrosion Products in PWR, BWR and SGHWR Systems", AERE-R 8164, United Kingdom Atomic Energy Authority Harwell, March 1976

2. T. J. Kabele and J. W. Bartlett, "Deposition of Iron Corrosion Products from an Aqueous Stream", Nucl. Eng. part XXI, Chem. Eng. Progress Symposium Series No. 104, Vol. 66, p. 12, 1970

3. D. H. Charlesworth, "The Deposition of Corrosion Products in Boiling Water Systems", Nucl. Eng. part XXI, Chemical Engineering Progress Symposium Series No. 104, Vol. 66, p. 21, 1970

4. S. K. Beal, "A Model of Crud and Radiation-Level Build-up in Reactor Plants", Trans. American Nuclear Society, Vol 17, 1973

5. G. C. W. Comley, "The Significance of Corrosion Products in Water Reactor Coolant Circuits", Nuclear Energy, Vol. 16, No. 1, pp. 41-72, 1985

6. J. Roesmer and M. W. Rootham, "Estimation of Activity Inventories in Primary Circuits of Pressurized Water Reactors", Water Chemistry of Nuclear Reactor Systems, BNES, London, pp. 187-193, 1978

7. P. V. Balakrishnan and G. M. Allison, "Some In-reactor Loop Experiments on Corrosion Product Transport and Water Chemistry", Nuclear Technology, Vol. 39, pp. 105-120, 1978

8. D. H. Lister, "The accumulation of Radioactive Corrosion Products in Nuclear Steam Generators", CORROSION-NACE, Vol. 35, No. 5, pp. 219-226, May 1979

9. T. Iwahori, T. Mizuno, and H. Koyama, "Role of Surface Chemistry in Crud Deposition on Heat Transfer Surface", CORROSION-NACE, Vol. 35, No. 8, pp. 345-350, August 1979

10. Y. Solomon and J. Roesmer, "Measurement of Fuel Element Crud Deposits in Pressurized Water Reactors", Nuclear Technology, Vol. 29, pp. 166-173, May

1976

11. Y. L. Sandler and R. H. Kunig, "The Solubility of Nonstoichiometric Nickel Ferrite in High-Temperature Aqueous Solution", Nuclear Science and Engineering, Vol. 64, pp. 866-874, 1977

12. D. H. Lister, "The Mechanisms of Corrosion Product Transport and Their Investigation in High Temperature Water Loops", CORROSION-NACE, Vol. 35, No. 3, pp. 89-96, March 1979

13. K. A. Burrill, "Corrosion Product Transport in Water-Cooled Nuclear Reactors; Part I: Pssurized Water Operation", The Canadian Journal of Chemical Engineering, Vol. 55, pp. 54-61, February 1977

14. P. V. Balakrishnan, "A Radiochemical Technique for the Study of Dissolution of Corroson Products in High Temperature Water", The Canadian Journal of Chemical Engineering, Vol. 55, pp. 357-360, June 1977

15. Y. L. Sandler, "Structure of PWR Primary Corrosion Products", CORROSION -NACE, Vl. 35, No. 5, pp. 205-208, May 1979

16. C. A. Bergmann, E. I. Landerman, D. R. Lorentz, D. D. Whyte, and M. D. Naughton, "Evaluation of Cobalt Sources in Westinghouse-Designed Three- and Four-Loop Plants", Electric Power Research Institute, NP-2681, October 1982

17. T. R. Young, J. T. LaDuca, T. E. Quattrochi, and M. Wiatrowski, "Cobalt Source Identification Program", Electric Power Research Institute, NP-2685, October 1982

18. D. A. Bridle, E. J. Bird, C. R. Mitchell, and C. J. Wood, "Cobalt Deposition in Oxide Films on Reactor Pipework", Electric Power Research Institute, NP-4499, March 1986

19. D. H. Lister, "The Transport of Radioactive Corrosion Products in High-Temperature Water; II. The activation of Isothermal Steel Surfaces", Nuclear Science and Engineering, Vol. 59, pp. 406-426, 1976

20. C. A. Bergmann and J. Roesmer, "Primary-side Deposits on the PWR Steam Generator Tubes", Electric Power Research Institute, NP-2968, 1983

21. D. A. Bridle, K. R. Butter, P. Cake, G. C. W. Comley, and C. R. Mitchell, "The Nature and Behavior of Particulates in PWR Primary Coolant", Electric Power Research Institute, NP-6640, December 1989

22. M. J. Song, Y. G. Chung, S. W. Shin, G. S. Lim, J. H. Han, and Y. H. Jung, "Development of Techniques for Reducing PWR Primary Coolant System Dose Rate", Korea Electric Power Research Institute, KRC-90N-J04, June 1993

23. D. H. Lister and R. D. Davidson, "Corrosion-Product Release in Light Water Reactors", Electric Power Research Institute, NP-6512, September 1989

24. B. E. Brown, H. H. Lu, and D. J. Duquette, "Effect of Flow Rates on Localized Corrosin Behavior of 304 Stainless Steel in Ozonated 0.5N NaCl", CORROSION-NACE, Vol. 48, No. 12, pp. 970-975, 1992

25. B. Poulson, "Advances in Understanding Hydrodynamic Effects on Corrosion", Corrosion Science, Vol. 35, No. 1-4, pp. 655-665, 1993

26. S. K. Beal, "Deposition of Particles in Turbulent Flow on Channel or Pipe Walls", Nuclear Science and Engineering, Vol. 40, pp. 1-11, 1970

27. D. H. Lister, "The Transport of Radioactive Corrosion Products in High-Temperature Water - I. Recirculating Loop Experiments", Nuclear Science and Engineering, Vol. 58, pp. 239-251, 1975

28. M. J. Driscoll, O. K. Harling, and G. E. Kohse, "In-Pile Loop Studies of the Effect of PWR Coolant pH on Corrosion Product Radionuclide Deposition", Electric Power Research Institute, TR-100156, February 1992

29. H. Ocken, "Surface Treatments to Reduce Radiation Fields; Test-Loop Studies and Plant Demonstrations", Electric Power Research Institute, NP-5209-SR, April 1988

30. D. H. Lister, P. G. Anderson, B. J. Barry, and R. G. Lavoie, "Deposition of Cobalt on Surface-Treated Stainless Steel Under PWR Conditions", Electric Power Research Institute, NP-6528, October 1989

31. R. H. Asay, O. Naudin, M. Thiry, B. Lantes, G. Gouillardou, P. Saurin and C. Weber, "Effect of Surface Treatments on Radiation Buildup in Steam Generator; Volume 1: Manway Seal Plate Tests in Chinon B1 PWR", Electric Power Research Institute, TR-100059, November 1991

32. G. T. Galbraith and D. J. Asay, "Chromium Coatings to Reduce Recontamination", Electric Power Research Institute, TR-102746, August 1993

WARNING: This Document contains information classified under U.S. Export Control regulations as restricted from export outside the United States. You are under an obligation to ensure that you have a legal right to obtain access to this information and to ensure that you obtain an export license prior to any re-export of this information. Special restrictions apply to access by anyone that is not a United States citizen or a Permanent United States resident. For further information regarding your obligations, please see the information contained below in the section titled "Export Control Restrictions."

Export Control Restrictions

Access to and use of EPRI Intellectual Property is granted with the specific understanding and requirement that responsibility for ensuring full compliance with all applicable U.S. and foreign export laws and regulations is being undertaken by you and your company. This includes an obligation to ensure that any individual receiving access hereunder who is not a U.S. citizen or permanent U.S. resident is permitted access under applicable U.S. and foreign export laws and regulations. In the event you are uncertain whether you or your company may lawfully obtain access to this EPRI Intellectual Property, you acknowledge that it is your obligation to consult with your company's legal counsel to determine whether this access is lawful. Although EPRI may make available on a case by case basis an informal assessment of the applicable U.S. export classification for specific EPRI Intellectual Property, you and your company acknowledge that this assessment is solely for informational purposes and not for reliance purposes. You and your company acknowledge that it is still the obligation of you and your company to make your own assessment of the applicable U.S. export classification and ensure compliance accordingly. You and your company understand and acknowledge your obligations to make a prompt report to EPRI and the appropriate authorities regarding any access to or use of EPRI Intellectual Property hereunder that may be in violation of applicable U.S. or foreign export laws or regulations.

About EPRI

EPRI creates science and technology solutions for the global energy and energy services industry. U.S. electric utilities established the Electric Power Research Institute in 1973 as a nonprofit research consortium for the benefit of utility members, their customers, and society. Now known simply as EPRI, the company provides a wide range of innovative products and services to more than 1000 energy-related organizations in 40 countries. EPRI's multidisciplinary team of scientists and engineers draws on a worldwide network of technical and business expertise to help solve today's toughest energy and environmental problems.

EPRI. Electrify the World

SINGLE USER LICENSE AGREEMENT

THIS IS A LEGALLY BINDING AGREEMENT BETWEEN YOU AND THE ELECTRIC POWER RESEARCH INSTITUTE, INC. (EPRI). PLEASE READ IT CAREFULLY BEFORE REMOVING THE WRAPPING MATERIAL.

BY OPENING THIS SEALED PACKAGE YOU ARE AGREEING TO THE TERMS OF THIS AGREEMENT. IF YOU DO NOT AGREE TO THE TERMS OF THIS AGREEMENT, PROMPTLY RETURN THE UNOPENED PACKAGE TO EPRI AND THE PURCHASE PRICE WILL BE REFUNDED.

1. GRANT OF LICENSE

EPRI grants you the nonexclusive and nontransferable right during the term of this agreement to use this package only for your own benefit and the benefit of your organization. This means that the following may use this package: (I) your company (at any site owned or operated by your company); (II) its subsidiaries or other related entities; and (III) a consultant to your company or related entities, if the consultant has entered into a contract agreeing not to disclose the package outside of its organization or to use the package for its own benefit or the benefit of any party other than your company.

This shrink-wrap license agreement is subordinate to the terms of the Master Utility License Agreement between most U.S. EPRI member utilities and EPRI. Any EPRI member utility that does not have a Master Utility License Agreement may get one on request.

2. COPYRIGHT

This package, including the information contained in it, is either licensed to EPRI or owned by EPRI and is protected by United States and international copyright laws. You may not, without the prior written permission of EPRI, reproduce, translate or modify this package, in any form, in whole or in part, or prepare any derivative work based on this package.

3. RESTRICTIONS

You may not rent, lease, license, disclose or give this package to any person or organization, or use the information contained in this package, for the benefit of any third party or for any purpose other than as specified above unless such use is with the prior written permission of EPRI. You agree to take all reasonable steps to prevent unauthorized disclosure or use of this package. Except as specified above, this agreement does not grant you any right to patents, copyrights, trade secrets, trade names, trademarks or any other intellectual property, rights or licenses in respect of this package.

4. TERM AND TERMINATION

This license and this agreement are effective until terminated. You may terminate them at any time by destroying this package. EPRI has the right to terminate the license and this agreement immediately if you fail to comply with any term or condition of this agreement. Upon any termination you may destroy this package, but all obligations of nondisclosure will remain in effect.

5. DISCLAIMER OF WARRANTIES AND LIMITATION OF LIABILITIES

NEITHER EPRI, ANY MEMBER OF EPRI, ANY COSPONSOR, NOR ANY PERSON OR ORGANIZATION ACTING ON BEHALF OF ANY OF THEM:

(A) MAKES ANY WARRANTY OR REPRESENTATION WHATSOEVER, EXPRESS OR IMPLIED, (I) WITH RESPECT TO THE USE OF ANY INFORMATION, APPARATUS, METHOD, PROCESS OR SIMILAR ITEM DISCLOSED IN THIS PACKAGE, INCLUDING MERCHANTABILITY AND FITNESS FOR A PARTICULAR PURPOSE, OR (II) THAT SUCH USE DOES NOT INFRINGE ON OR INTERFERE WITH PRIVATELY OWNED RIGHTS, INCLUDING ANY PARTY'S INTELLECTUAL PROPERTY, OR (III) THAT THIS PACKAGE IS SUITABLE TO ANY PARTICULAR USER'S CIRCUMSTANCE; OR

(B) ASSUMES RESPONSIBILITY FOR ANY DAMAGES OR OTHER LIABILITY WHATSOEVER (INCLUDING ANY CONSEQUENTIAL DAMAGES, EVEN IF EPRI OR ANY EPRI REPRESENTATIVE HAS BEEN ADVISED OF THE POSSIBILITY OF SUCH DAMAGES) RESULTING FROM YOUR SELECTION OR USE OF THIS PACKAGE OR ANY INFORMATION, APPARATUS, METHOD, PROCESS OR SIMILAR ITEM DISCLOSED IN THIS PACKAGE.

6. EXPORT

The laws and regulations of the United States restrict the export and re-export of any portion of this package, and you agree not to export or re-export this package or any related technical data in any form without the appropriate United States and foreign government approvals.

7. CHOICE OF LAW

This agreement will be governed by the laws of the State of California as applied to transactions taking place entirely in California between California residents.

8. INTEGRATION

You have read and understand this agreement, and acknowledge that it is the final, complete and exclusive agreement between you and EPRI concerning its subject matter, superseding any prior related understanding or agreement. No waiver, variation or different terms of this agreement will be enforceable against EPRI unless EPRI gives its prior written consent, signed by an officer of EPRI.

Program:

Nuclear Power

TR-109006

EPRI • 3412 Hillview Avenue, Palo Alto, California 94304 • PO Box 10412, Palo Alto, California 94303 • USA
800.313.3774 • 650.855.2121 • askepri@epri.com • www.epri.com